Supplementary Materials

Solvothermal synthesis and formation mechanism of lithium dodecaborate

Jian Wang[1,2], Timothy Steenhaut[1], Koen Robeyns[1], Hai-Wen Li[2,*], Yaroslav Filinchuk[1,*]

[1]Institute of Condensed Matter and Nanosciences, Université catholique de Louvain, Louvain-la-Neuve 1348, Belgium.
[2]School of Advanced Energy, Sun Yat-sen University, Shenzhen 518107, Guangdong, China.

[*]**Correspondence to:** Prof. Hai-Wen Li, School of Advanced Energy, Sun Yat-sen University, Shenzhen 518107, Guangdong, China. E-mail: lihw76@mail.sysu.edu.cn; Prof. Yaroslav Filinchuk, Institute of Condensed Matter and Nanosciences, Université catholique de Louvain, Louvain-la-Neuve 1348, Belgium. E-mail: yaroslav.filinchuk@uclouvain.be

1 Experimental Section

1.1 Chemicals

Lithium borohydride ($LiBH_4$, anhydrous, 95%), sodium borohydride ($NaBH_4$, anhydrous, 95 %), potassium borohydride (KBH_4, anhydrous, 98 %), borane dimethyl sulfide complex (~10-10.2 M, $(CH_3)_2S{\cdot}BH_3$, BMS, analytical), borane tetrahydrofuran complex solution ($THF{\cdot}BH_3$, 1 M in THF, <0.005 M sodium borohydride as stabilizer), diethylene glycol dimethyl ether (diglyme, $C_6H_{14}O_3$, anhydrous, 99.5%), 1,2-Dimethoxyethane (monoglyme, DME, $C_4H_{10}O_2$, anhydrous, 99.5%), dimethyl sulfoxide (DMSO, anhydrous, 99.9%), *N*,*N*-Diethylformamide ($C_5H_{11}NO$, DEF, 99%), toluene (C_7H_8, 99.85%) and dichloromethane (CH_2Cl_2, 99.8%) were obtained from Sigma-Aldrich. Deuterated dimethyl sulfoxide (DMSO-d_6, 99.9 atom % D), deuterated dimethyl sulfoxide with TMS (DMSO-d_6 with TMS (0.03 vol.%), 99.8 atom % D), deuterated acetonitrile (CD_3CN-d_3, 99.8 atom % D), deuterated tetrahydrofuran, (THF-d_8, 99.5 atom % D) and deuterated dichloromethane (CD_2Cl_2, 99.8 atom % D) were obtained from Eurisotop. All the above chemicals were used without further purification.

1.2 Characterization

1.2.1 NMR Spectroscopy

All NMR spectra were acquired on a Bruker Avance 500 spectrometer (^1H: 500.13 MHz, ^{11}B:160.46 MHz) at room temperature, utilizing a {^1H, X} probe head fitted with a *z*-gradient coil. The TopSpin 1.3 software (Bruker) was employed to run the experiments. Unless state otherwise, solid samples were dissolved and filtrates diluted (0.35 ml of filtrate mixed with 0.2 ml of DMSO-d_6; the NMR samples containing filtrates were prepared under Ar protection) in deuterated DMSO (alternatively deuterated acetonitrile was used for samples in which DMSO was quantified). ^1H chemical shifts were calibrated using the residual peaks of the deuterated solvents (δ = 2.50 ppm for DMSO-d_6, 1.94 ppm for CD_3CN-d_3) or TMS internal standard (δ = 0 ppm). External referencing to $BF_3{\cdot}Et_2O$ (δ = 0.00 ppm) was performed for the ^{11}B NMR signals. All experiments were carried out using quartz NMR tubes with an internal diameter of 5 mm. The splitting patterns in NMR spectra are reported as follows: s = singlet; d = doublet; t = triplet; m = multiplet.

NMR assignments:

^{1}H NMR (DMSO-d_6, 500.13 MHz):

$B_{12}H_{12}^{2-}$: δ (ppm) = 0 to 1.50 (m, 12H, $B^{1-12}H$);

Diglyme ($C_6H_{14}O_3$): δ (ppm) = 3.23 (s, 6H, OCH_3), 3.43 (m, 4H, CH_2) and 3.49 (m, 4H, CH_2);

Monoglyme ($C_4H_{10}O_2$): δ (ppm) = 3.23 (s, 6H, OCH_3), 3.42 (s, 4H, CH_2);

H_2O: δ (ppm) = 3.31 to 3.39 (s, 2H, OH);

DMSO: δ (ppm) = 2.54 (s, 6H, OCH_3);

TMS: δ (ppm) = 0.00 (s, 12H, $SiCH_3$).

^{11}B NMR (DMSO-d_6, 160.46 MHz):

$B_{12}H_{12}^{2-}$: δ (ppm) = −15.22 (d, $B^{1\text{-}12}H$, J = 125.4 Hz);

$B_{12}H_{12\text{-}x}^{2-}$: δ (ppm) = 6.78(s, BO); −16.50 (d, J = 126.2 Hz), −18.03 (d, J = 120.0 Hz), −22.91 (d, J = 129.0 Hz);

$B_{10}H_{10}^{2-}$: δ (ppm) = −0.56 (d, $B^{1,10}H$, J = 137.2 Hz), −28.38 (d, $B^{2-9}H$, J = 128.7 Hz);

$B_{11}H_{14}^{-}$: δ (ppm) = −13.83 (d, $B^{1}H$, J = 139.4 Hz), −16.06 (t, $B^{2-11}H$, J = 129.7 Hz);

$B_{10}H_{13}^{-}$: δ (ppm) = 6.85 (d, $B^{6,9}H$), 2.69 (d, $B^{1(3)}H$); −4.73 (d, $B^{5,7,8,10}H$), −34.98 (d, $B^{2,4}H$, signal too broad to distinguish coupling);

$B_9H_{14}^{-}$: δ (ppm) = −8.08 (d, $B^{5,7,9}H$ J = 144.4 Hz), −20.29 (d, $B^{4,6,8}H$, J = 113.6 Hz); −23.63 (d, $B^{1,2,3}H$ J = 159.3 Hz);

$B_3H_8^{-}$: δ (ppm) = −29.2 (n, J = 33.5 Hz);

$B_2H_7^{-}$: δ (ppm) = −24.54 (quartet of doublets);

BH_4^{-}: δ (ppm) = −35.23 (q, J = 81.8 Hz);

$B(OH)_4^{-}$: δ (ppm)= 1.95 (s);

$DMS{\cdot}BH_3$: δ (ppm)= −19.89 (q);

$DMSO{\cdot}BH_3$: δ (ppm)= −6.23 (q).

1.2.2 Powder X-ray Diffraction (PXRD)

Standard and *in situ* laboratory powder X-ray diffraction experiments were performed on a MAR345 image plate detector, with Mo Kα radiation (λ = 0.71073 Å) generated by an Incoatec Microfocus Source Mo ELM47 operating at 50 kV and 1000 µA. The powdered samples were loaded inside thin-walled glass capillaries (0.7 mm diameter, Hilgenberg, GmbH) which were sealed with grease under the protective atmosphere of an argon-filled glovebox. After being removed from the glovebox, the capillaries were cut and promptly placed into molten wax on goniometric heads, followed by immediate

measurements to prevent sample degradation. Samples were rotated by 180° during a 10-minute exposure. For in-situ powder X-ray diffraction, the samples underwent a 60° rotation over a 10-minute exposure period. The procedure involved heating the capillary containing the sample, utilizing a Leister LE MINI SENSOR KIT hot air blower from Leister Technologies Benelux B.V. The air blower was calibrated using a thermocouple housed in a capillary (the determined error in sample temperature was ±5 °C). Data were integrated using the Fit2D software (ESRF), using LaB_6 as calibrant.

1.2.3 Single-Crystal X-ray Diffraction

The single crystal X-Ray diffraction data were acquired on a MAR345 image plate detector using Mo Kα radiation (λ= 0.71073 Å), either at ambient temperature or after flash cooling to 150 K in a nitrogen gas stream. Data indexation, integration and reduction was done with the CrysAlis^{PRO} software, incorporating an empirical absorption correction. Structures were solved by dual space direct methods (SHELXT), followed by refinement using full-matrix least squares based on $|F^2|$ with SHELXL 2018/ 3. Non-hydrogen atoms were anisotropically refined, while hydrogen atoms were positioned at calculated positions and refined in riding mode, with temperature factors constrained to 1.2 times Ueq of the parent atoms (1.5 times Ueq for methyl and OH hydrogens. The Vesta software was used to generate figures of crystal structures.

1.2.4 Synchrotron Radiation Powder X-ray Diffraction (SR-PXRD)

Single scan and *in situ* synchrotron radiation powder X-ray diffraction (SR-PXRD) data were collected at the Swiss-Norwegian beamline BM01 at the European Synchrotron Radiation Facility (ESRF) in Grenoble, using the PILATUS@SNBL diffractometer, which is equipped with a Dectris PILATUS 2M single-photon counting pixel area detector (λ = 0.77509 Å). Raw data were processed through the SNBL Toolbox software to generate powder patterns, using a LaB_6 standard for refining experimental parameters.

1.2.5 Attenuated Total Reflectance Fourier Transform Infrared Spectroscopy (ATR-FTIR)

Attenuated total reflectance Fourier transform infrared (ATR-FTIR) spectra were obtained using a Bruker Alpha II spectrometer housed in an argon-filled glovebox. The

spectrometer was equipped with a Platinum ATR module (Bruker, diamond crystal, single bounce) for measurements. Each spectrum was recorded within the 370-4000 cm^{-1} range at a resolution of 4 cm^{-1}, averaged over 24 scans.

1.2.6 Thermogravimetry/Differential Scanning Calorimetry analyses

Thermogravimetric analysis/differential scanning calorimetry (TGA/DSC) was carried out using a NETZSCH STA 449 F3 Jupiter instrument equipped with a stainless-steel oven housed within an argon-filled glovebox. Measurements were conducted at a heating rate of 5 K/min under a constant Ar flow (total flow of 100 mL/min), spanning a temperature range of 25 to 500 °C. Alternatively, the TGA measurement to evaluate the thermal stability of $Li_2B_{12}H_{12}$·n diglyme (sample S6) was conducted on a Mettler Toledo TGA/DSC 3+ system equipped with a sample robot. A nitrogen (N_2) flow rate of 100 mL/min was used for the measurement. Prior to heating, an initial isotherm at 27 °C was maintained for 15 minutes, and the sample was then heated to 500 °C at a rate of 10 K/min.

1.2.7 Ball milling

Ball-milled $LiBH_4$ ($NaBH_4$) was produced by mechanically milling 1.0 g of borohydrides at room temperature using a planetary ball mill (Fritsch Pulverisette P7). Four steel balls (10 mm in diameter) were loaded into a hardened steel vial (30 cm^3 in volume) in an argon-filled glovebox. Milling was conducted under 0.1 MPa of Ar (2 min of milling cycles, 3 min of pausing, 24 cycles).

1.3 Syntheses

General comment: The syntheses were either conducted in a 100 mL Schlenk flask equipped with a fritted glass P4 porosity filtration disk (see Supplementary Figures 1, 2 and 3) or in a stainless-steel autoclave (Anhui Kemi Instrument Co., Ltd.; volume of 50 mL, equipped with a 37.5 ml quartz liner).[1] The weighing error for borohydrides was maintained within ± 0.002 g. A 10% excess of $DMS{\cdot}BH_3$ was employed in both autoclave and Schlenk conditions to compensate for evaporative losses.

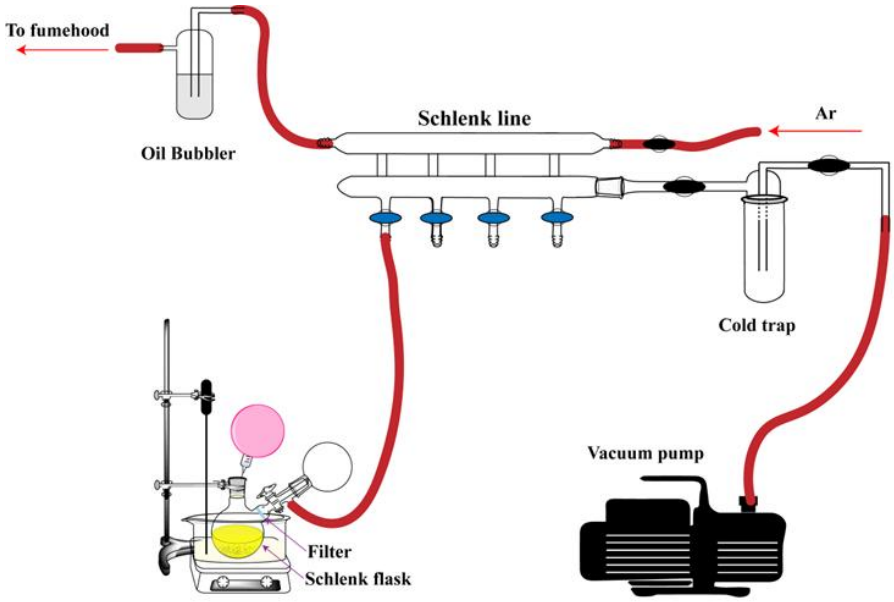

Supplementary Figure 1. Scheme of the complete Schlenk line setup used for the synthesis of $B_{12}H_{12}^{2-}$.

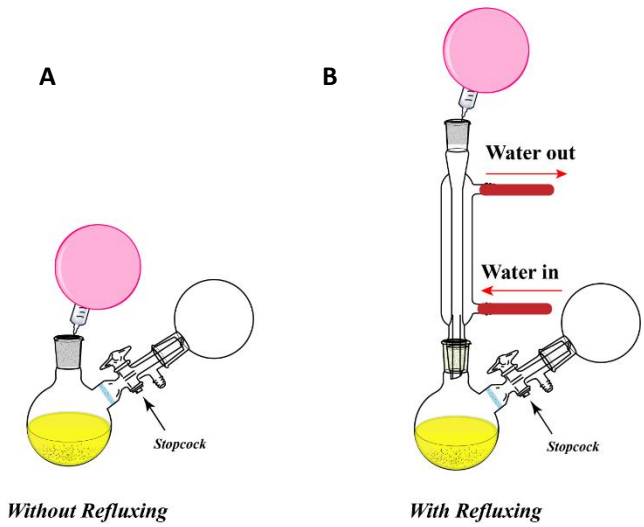

Supplementary Figure 2. Scheme of the Schlenk setup used for $B_{12}H_{12}^{2-}$ synthesis (A) without or (B) with refluxing.

Note: During the synthesis the stopcock of the setup is maintained in closed state, and it is opened only for the filtration and washing steps.

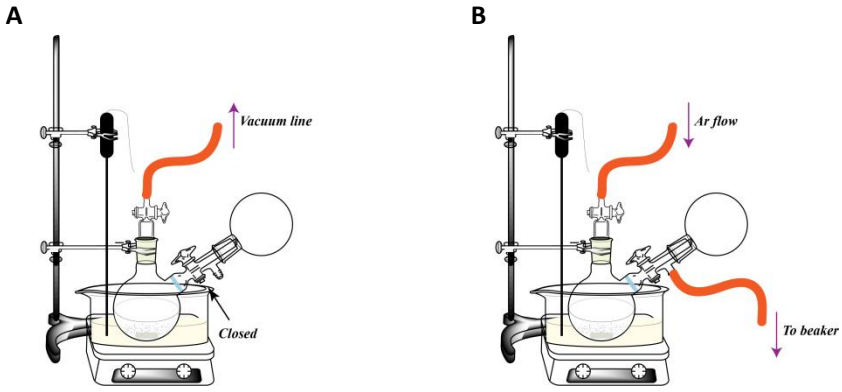

Supplementary Figure 3. Scheme of the Schlenk setup used for $B_{12}H_{12}^{2-}$ synthesis and thermal desolvation (A) under vacuum or (B) under argon flow.

Note: During the thermal removal of solvents, we used a piece of aluminum paper to cover the upper part of the Schlenk flask to ensure homogeneous heating, including the portion of the flask outside the oil bath.

1.3.1 Synthesis of $Na_2B_{12}H_{12}$ and $K_2B_{12}H_{12}$ in Schlenk flask under reflux

$NaBH_4$ (0.19 g, 5 mmol) or KBH_4 (0.27 g, 5 mmol) was accurately weighed and added to a 100 mL Schlenk flask equipped with a glass frit within an Ar-filled glovebox. The flask was then connected to a Schlenk line and an Ar-purged condenser outside the glovebox (Supplementary Figure 2B). Subsequently, 20 mL of diglyme and 27.5 mmol (2.75 mL) of borane dimethyl sulfide complex $(CH_3)_2S{\cdot}BH_3$ were added to the borohydride and the reaction solution was stirred at 160 °C for 24 hours. The reaction mixture was then cooled to room temperature and filtered using the Schlenk filtration apparatus incorporated in the reaction setup (Supplementary Figure 2B) and washed with diglyme (3 x 5 mL). The obtained sample was dried at 80 °C under vacuum for 4 hours to convert the sticky powders into unsolvated products. The resulting raw product was obtained as a white substance. The yield of $Na_2B_{12}H_{12}$ was approximately 92% and that of $K_2B_{12}H_{12}$ was around 88%, based on the amount of $NaBH_4$ (KBH_4) in use.

1.3.2 Synthesis of anhydrous $Li_2B_{12}H_{12}$ in toluene

0.11 g of $LiBH_4$ (or ball-milled $LiBH_4$, 5 mmol) was weighed into the quartz liner reactor (or Schlenk flask) in a glovebox. 20 mL of toluene was added, followed by 27.5 mmol of the borane dimethyl sulfide complex ($(CH_3)_2S{\cdot}BH_3$, 2.75 mL), and the reaction solution was stirred at 120 °C for 24 hours. The reaction mixture was then

cooled to room temperature, filtered using the Schlenk filtration apparatus incorporated in the reaction setup (Supplementary Figure 2B), washed with toluene (3 ×5 mL), and then dried at 50°C under vacuum for 2 h.

1.3.3 Isolation of $LiB_{11}H_{14}$

$LiBH_4$ (0.11 g, 5 mmol) was accurately weighed and introduced into a 100 mL Schlenk flask equipped with a glass frit within an Ar-filled glovebox. The flask was then connected to a Schlenk line and a condenser outside the glovebox (Supplementary Figure 2A), and the system was quickly purged with argon. Subsequently, 20 mL of diglyme and 27.5 mmol (2.75 mL) of borane dimethyl sulfide complex ($(CH_3)_2S{\cdot}BH_3$) were added to the borohydride, and the reaction solution was stirred at 120 °C (85 °C) for 24 hours. The reaction mixture was then cooled to room temperature and filtered using the Schlenk filtration apparatus incorporated in the reaction setup (Supplementary Figure 2A). At this stage, the obtained solid sample was diglyme-solvated $Li_2B_{12}H_{12}$. $B_3H_8^-$, $B_9H_{14}^-$ and $B_{11}H_{14}^-$ were the main components in the yellow solution resulting from the filtration. Heating this isolated solution at 160 °C for 4 h allowed to obtain a second batch of solid $Li_2B_{12}H_{12}$, by conversion of the dissolved species into a precipitate that was recovered after cooling to room temperature and a second filtration using the Schlenk filtration apparatus incorporated in the reaction setup (Supplementary Figure 2B). At this stage, $B_{11}H_{14}^-$ remained as main species in the yellow solution collected from the filtration, and solvated $LiB_{11}H_{14}$ was obtained as a yellow oily product after diglyme evaporation at 160 °C under Ar flow using the Schlenk setup in Supplementary Figure 3B.

Supplementary Table 1. Reported solubilities of alkali borohydrides in the solvents used in this work (at 25 °C).[2]

Description	**$LiBH_4$**	**$NaBH_4$**	**KBH_4**
Diglyme	9.64g / 100g (4.25M)	5.5g / 100g	Insoluble
Monoglyme	9.81g / 100g (4.7M)	0.8g / 100g	n.d.
Toluene	Insoluble	Insoluble	Insoluble
DMSO	soluble	soluble	7.6 g / 100g

2 Effect of the $LiBH_4$ / $DMS{\cdot}BH_3$ ratio used for the Schlenk flask synthesis of $Li_2B_{12}H_{12}$ in diglyme

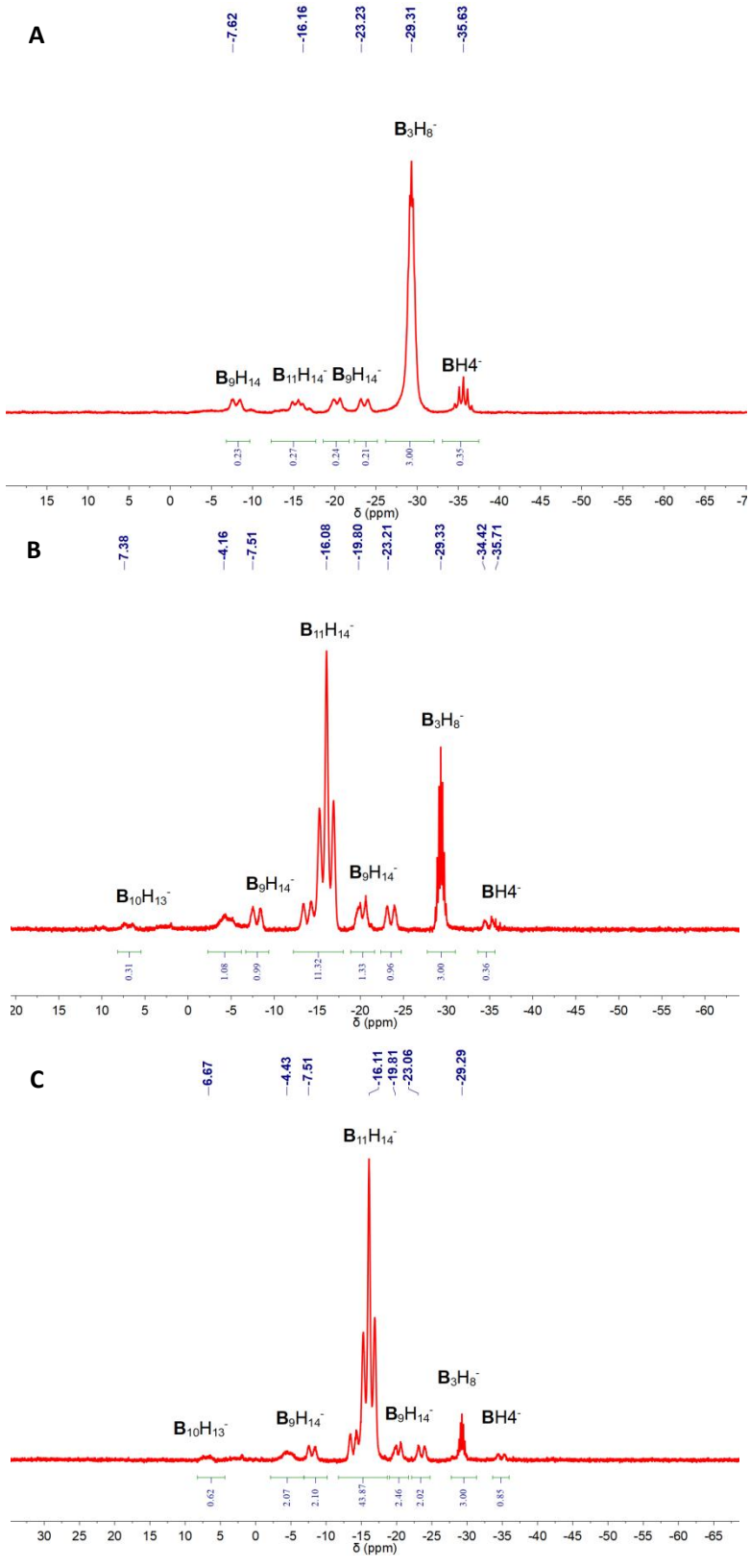

Supplementary Figure 4. Integrated proton-coupled ^{11}B NMR spectra of filtrates obtained from Schlenk flask syntheses of $Li_2B_{12}H_{12}$ using different $LiBH_4$ / $DMS{\cdot}BH_3$

ratios: (A) $LiBH_4$: $DMS{\cdot}BH_3$ = 1: 2 (using 5 mmol $LiBH_4$ and 10 mmol $DMS{\cdot}BH_3$), (B) $LiBH_4$: $DMS{\cdot}BH_3$ = 1: 5.5 (using 27.5 mmol $DMS{\cdot}BH_3$) and (C) $LiBH_4$: $DMS{\cdot}BH_3$= 1: 10 (using 50 mmol $DMS{\cdot}BH_3$).

Supplementary Table 2. Composition of filtrates obtained from experiments using different $LiBH_4$: BMS ratios, as determined from the NMR spectra in Supplementary Figure 4.

Description	**$LiBH_4$: BMS ratio**	**Composition (molar ratio relative to $B_3H_8^-$)**				
		BH_4^-	**$B_3H_8^-$**	**$B_9H_{14}^-$**	**$B_{10}H_{13}^-$**	**$B_{11}H_{14}^-$**
a	1: 2	0.35	1	0.23	n.d.	0.07
b*	1: 5.5	n.d.	1	0.36	0.175	1.03
c	1: 10	n.d.	1	0.73	0.355	3.98

*Note: for the filtrate b, the signals originating from small clusters were overlapped, as observed in the $^{11}B\{^1H\}$ spectrum (Supplementary Figure 4B). This suggests that BH_4^- and $B_2H_7^-$ coexist in the filtrate, with a slight residual amount of $B_{12}H_{12}^{2-}$, leading to a potentially substantial error in the integration of the signal of $B_{11}H_{14}^-$.

3 Effect of reaction temperature on the synthesis of $Li_2B_{12}H_{12}$ in diglyme

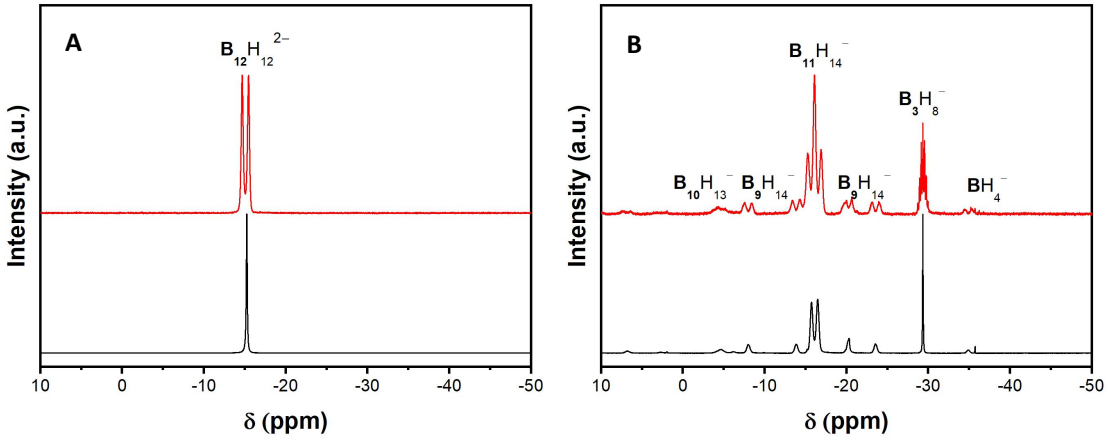

Supplementary Figure 5. Proton-decoupled (black) and coupled (red) ^{11}B NMR spectra of (A) solid precipitate and (B) filtrate of after reaction of $LiBH_4$ with 5 equiv (10% excess) of $DMS{\cdot}BH_3$ for 24 hours at 120°C in a Schlenk flask.

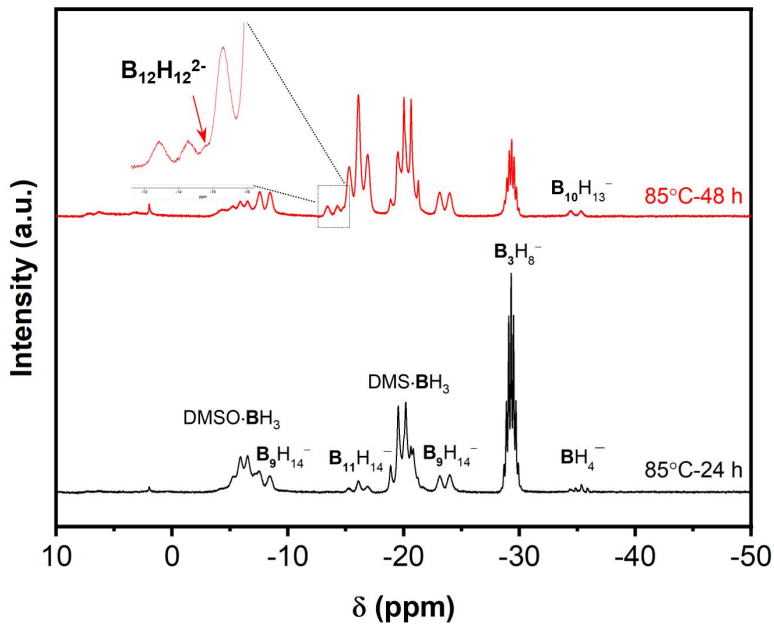

Supplementary Figure 6. Proton-coupled ^{11}B NMR spectra of mixture containing $LiBH_4$ with 5 equiv (10% excess) of $DMS{\cdot}BH_3$ after 24 hours (black) and 48 hours (red) of reaction at 85 °C in a Schlenk flask.

4 Comparison of the synthesis in Schlenk flask with and without condenser

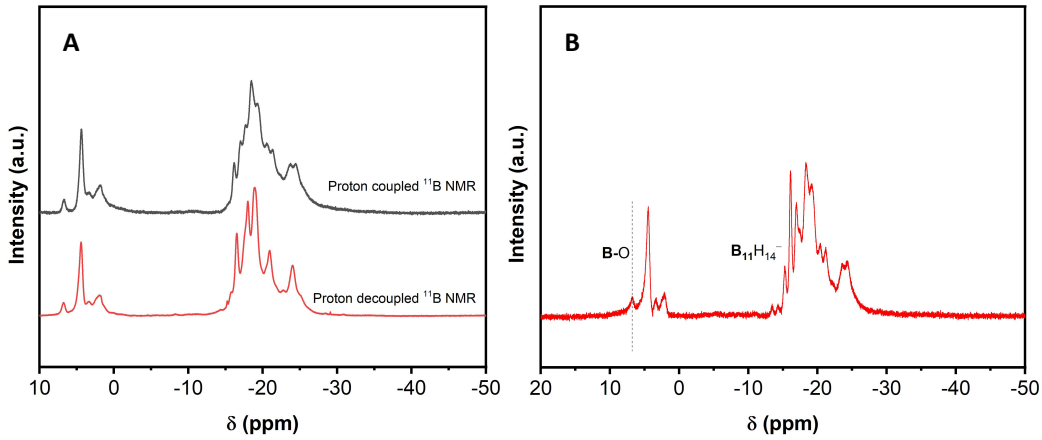

Supplementary Figure 7. (A) Proton-coupled and decoupled ^{11}B NMR spectra of yellow oily residue obtained upon reaction of $LiBH_4$ with 5 equiv (10% excess) of $DMS{\cdot}BH_3$ for 24 hours at 160 °C in a Schlenk flask without condenser and (B) ^{11}B NMR spectrum of the filtrate diluted in DMSO-d_6. The reaction at 160°C leads to partial dehydrogenation of $Li_2B_{12}H_{12}{\cdot}n$ diglyme (diglyme = $C_6H_{14}O_3$), forming $Li_2B_{12}H_{12-x}{\cdot}n\ C_6H_{14-x}O_3$.

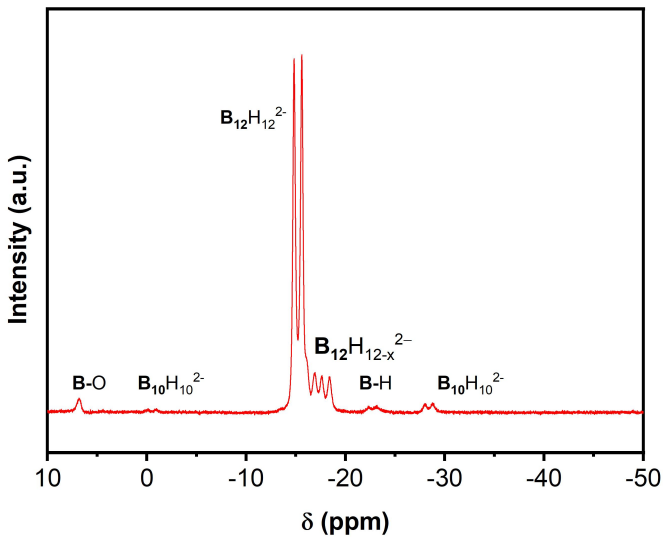

Supplementary Figure 8. Proton-coupled ^{11}B NMR spectrum of the solid precipitate obtained upon reacting $LiBH_4$ with 5 equiv (10% excess) of $DMS{\cdot}BH_3$ for 24 hours at 160 °C in a Schlenk flask equipped with a condenser. The reaction at 160°C leads to partial dehydrogenation of $Li_2B_{12}H_{12}{\cdot}n$ diglyme (diglyme = $C_6H_{14}O_3$), forming $Li_2B_{12}H_{12-x}{\cdot}\ n\ C_6H_{14-x}O_3$.

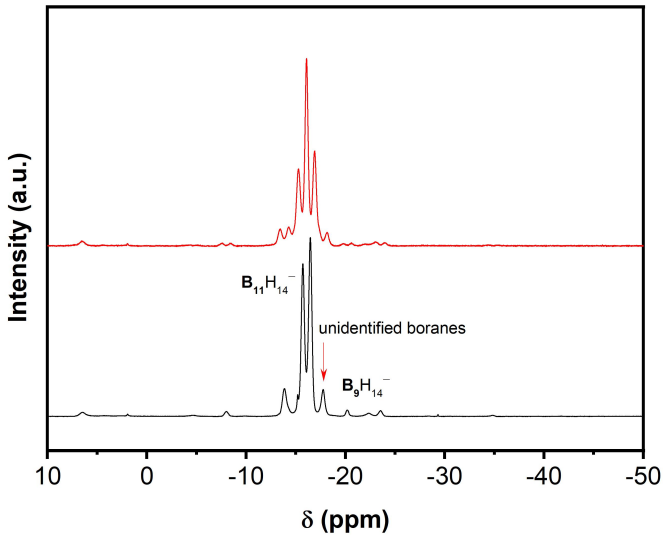

Supplementary Figure 9. Proton-decoupled (black) and coupled (red) ^{11}B NMR spectra of a filtration obtained upon reacting $LiBH_4$ with 5 equiv. (10% excess) of $DMS{\cdot}BH_3$ for 24 hours at 120 °C in a Schlenk flask equipped with a condenser.

Note: Conducting the synthesis in a setup equipped with a condenser facilitated the dehydrocondensation reaction of lower borane clusters, resulting in the formation of $B_{11}H_{14}^-$. Additionally, the presence of partially dehydrogenated $Li_2B_{12}H_{12-x}{\cdot}n\ C_6H_{14-x}O_3$ anions can also be attributed to the presence of traces of H_2O in the solvents used in the process.

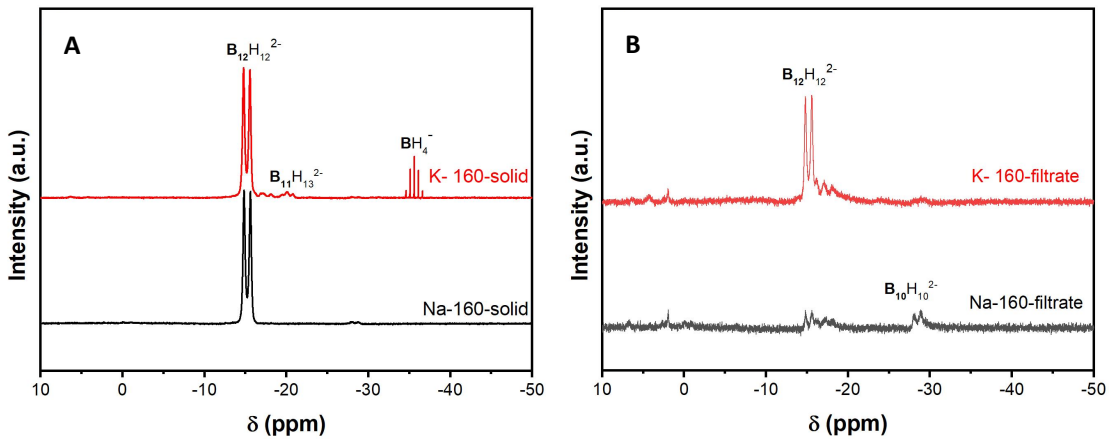

Supplementary Figure 10. Proton-coupled ^{11}B NMR spectra of (A) solid precipitates and (B) filtrates obtained upon reaction of 5 mmol $NaBH_4$ (black) and KBH_4 (red) with 5 equiv (10% excess) of $DMS{\cdot}BH_3$ for 24 hours at 160°C in a Schlenk setup in refluxing diglyme.

5 Calculation of the yields of isolated $Li_2B_{12}H_{12}$ obtained from syntheses in Schlenk flask and in autoclave

Supplementary Table 3. Yields of $Li_2B_{12}H_{12}$ isolated from the reaction of $LiBH_4$ and BMS in a Schlenk flask under various conditions.

Entry (*)	Reagents			Reaction conditions		Crude sample weight after drying	Composition of precipitates based on ^1H NMR	Yield of $Li_2B_{12}H_{12}$
	$LiBH_4$ (mmol)	$DMS{\cdot}BH_3$ (mmol)	Diglyme (ml)	Temp (°C)	Time (h)	(g)		(%)
S1	5	27.5	20	85	24/48	Uncollectible	/	< 5
S2	5	10	20	120	24	0.19	$Li_2B_{12}H_{12}$ + 4.07 diglyme	11
S3	5	50	20	120	24	0.32	$Li_2B_{12}H_{12}$ + 2.8 diglyme	25
S4	5	27.5	20	120	12	0.47	$Li_2B_{12}H_{12}$ + 3.73 diglyme	30
S5	5	27.5	20	120	24	0.68	$Li_2B_{12}H_{12}$ + 3.57 diglyme	45
S6	10	55	20	120	24	0.88	$Li_2B_{12}H_{12}$ + 2.28 diglyme	40
S7	5	27.5	20	120 (Refluxing)	24	0.52	$Li_2B_{12}H_{12}$ + 2.24 diglyme	48
S8	5	27.5	20	120	48	0.92	$Li_2B_{12}H_{12}$ + 4.18 diglyme	54
S9	5	27.5	20	160	24	Yellow oily compound	unidentified boranes; $B_{11}H_{14}^-$; $B_{12}H_{12-x}^{2-}$	
S10	5	27.5	20	160 (Refluxing)	24	1.46	$B_{12}H_{12}^{2-}$; $B_{10}H_{10}^{2-}$; $B_{12}H_{12-x}^{2-}$	

Supplementary Table 4. Isolated yields from the reactions between $NaBH_4$ (KBH_4) and $DMS{\cdot}BH_3$ in refluxing diglyme.

Entry (*)	Reagents			Reaction conditions		Crude sample weight after drying	Composition of precipitate based on ^1H NMR	Yield of $M_2B_{12}H_{12}$ (M = Na or K) (%)
	BH_4^- (mmol)	$DMS{\cdot}BH_3$ (mmol)	Diglyme (ml)	Temp (°C)	Time (h)			
$NaBH_4$	5	27.5	20	160	24	0.98 g	$Na_2B_{12}H_{12}$ + 1.76 diglyme	92
KBH_4*	5	27.5	20	160	24	0.5 g	$K_2B_{12}H_{12}$	88

* The sample contains ~5 % $K_2B_{12}H_{12-x}{\cdot}$ n $C_6H_{14-x}O_3$ impurities after purification, based on integration of the ^{11}B NMR spectrum.

Supplementary Table 5. Yields of $Li_2B_{12}H_{12}$ isolated from the reaction of $LiBH_4$ and BMS in an autoclave under various conditions.

Entry (*)	Reagents			Reaction conditions		Crude sample weight after drying	Composition of precipitates based on ^1H NMR	Yield of $Li_2B_{12}H_{12}$
	$LiBH_4$ (mmol)	$DMS{\cdot}BH_3$ (mmol)	Diglyme (ml)	Temp (°C)	Time (h)	(g)		(%)
A1	5	27.5	20	120	12	0.94	$Li_2B_{12}H_{12}$ + 3.31 diglyme	66
A2	5	27.5	20	120	24	1.13	$Li_2B_{12}H_{12}$ + 2.75 diglyme	91
A3	5	27.5	20	120	48	1.44	$Li_2B_{12}H_{12}$ + 3.54 diglyme	96
A4	10	55	20	120	24	2.81	$Li_2B_{12}H_{12}$ + 3.99 diglyme	86
A5	5	55	20	160	24	Colorless oily compound	unknown boranes	

Supplementary Table 6. Yields of $Li_2B_{12}H_{12}$ isolated from the reaction of $LiBH_4$ and BMS in monoglyme in an autoclave.

Entry (*)	Reagents			Reaction conditions		Crude sample weight after drying	Composition of precipitates based on ^1H NMR	Yield of $Li_2B_{12}H_{12}$
	$LiBH_4$ (mmol)	$DMS{\cdot}BH_3$ (mmol)	monoglyme (ml)	Temp (°C)	Time (h)	(g)		(%)
A6*	10	55	20	120	24	1.38	$Li_2B_{12}H_{12}$ + 5.92 monoglyme	42
A7	10	55	20	120	24	1.42	$Li_2B_{12}H_{12}$ + 1.99 monoglyme	89

* The particle size of A6 was too small to allow filtration (below 16 μm), solid precipitates remained in the filtrate

The calculation of yields is based on equation (1) below:

$$2\ MBH_4 + 10\ (CH_3)_2S{\cdot}BH_3 \rightarrow M_2B_{12}H_{12} + 10\ (CH_3)_2S + 13\ H_2 \quad (M= Li, Na, K) \qquad (1)$$

The theoretical yields of $M_2B_{12}H_{12}$ from 5 mmol MBH_4 (M = Li, Na, K), which is the typical amount used in the experiments, are listed in Supplementary Table 7 below:

Supplementary Table 7. Theoretical yields of $M_2B_{12}H_{12}$ from 5 mmol MBH_4 (M = Li, Na, K).

MBH_4	Weight (g)	Purity (%)	Theoretical yields of $M_2B_{12}H_{12}$ (g)
$LiBH_4$	0.11	95	0.37
$NaBH_4$	0.19	95	0.45
KBH_4	0.27	98	0.54

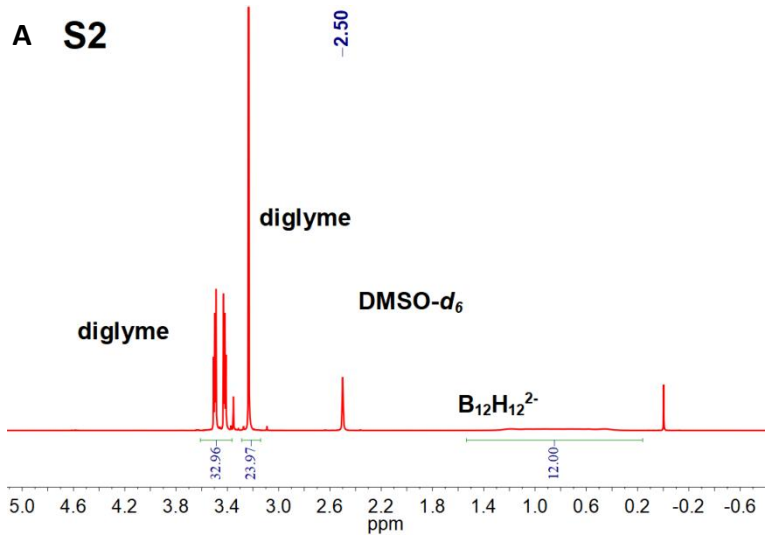
A
S2
2.50
diglyme
DMSO-d_6
diglyme
$B_{12}H_{12}^{2-}$
32.96
23.97
12.00
5.0 4.6 4.2 3.8 3.4 3.0 2.6 2.2 1.8 1.4 1.0 0.6 0.2 -0.2 -0.6
ppm

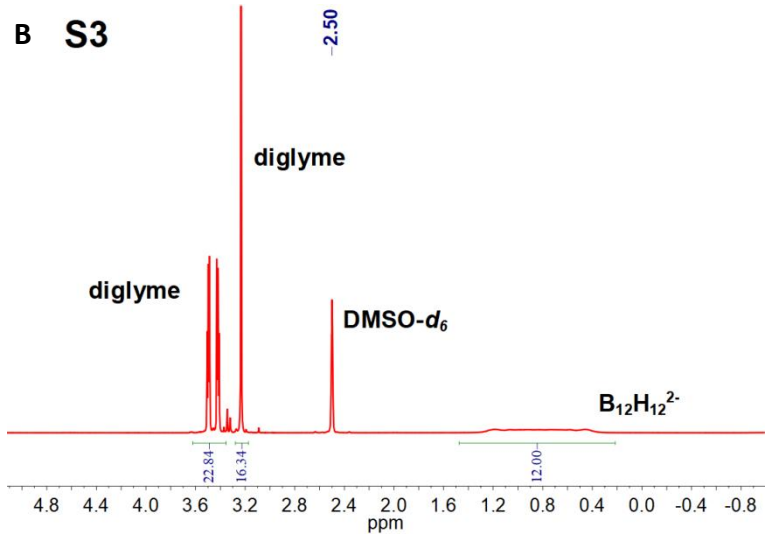
B
S3
2.50
diglyme
diglyme
DMSO-d_6
$B_{12}H_{12}^{2-}$
22.84
16.34
12.00
4.8 4.4 4.0 3.6 3.2 2.8 2.4 2.0 1.6 1.2 0.8 0.4 0.0 -0.4 -0.8
ppm

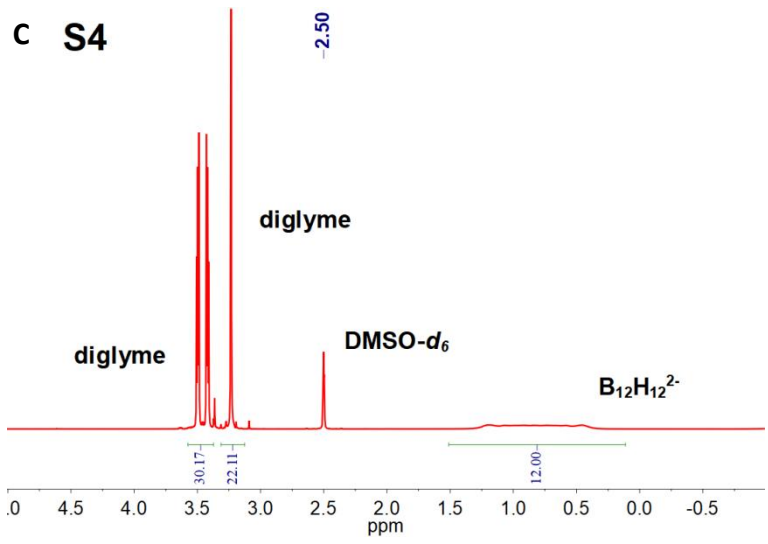
C
S4
2.50
diglyme
diglyme
DMSO-d_6
$B_{12}H_{12}^{2-}$
30.17
22.11
12.00
.0 4.5 4.0 3.5 3.0 2.5 2.0 1.5 1.0 0.5 0.0 -0.5
ppm

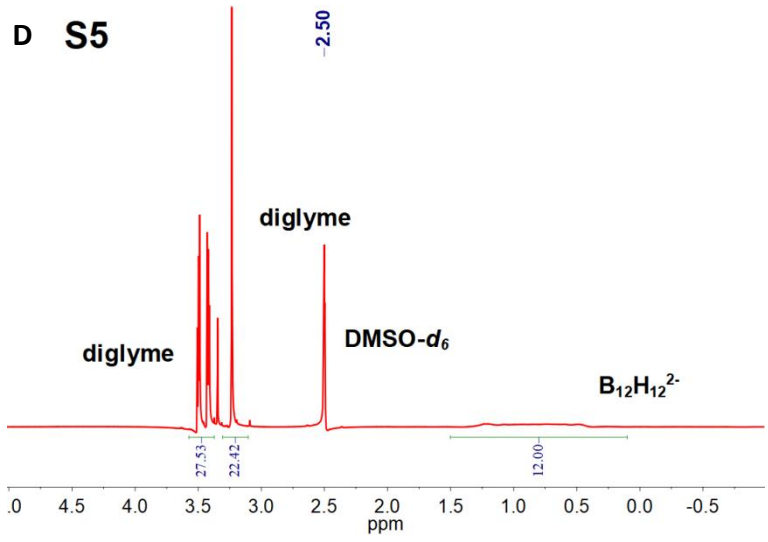
D
S5
2.50
diglyme
diglyme
DMSO-d_6
$B_{12}H_{12}^{2-}$
27.53
22.42
12.00
.0 4.5 4.0 3.5 3.0 2.5 2.0 1.5 1.0 0.5 0.0 -0.5
ppm

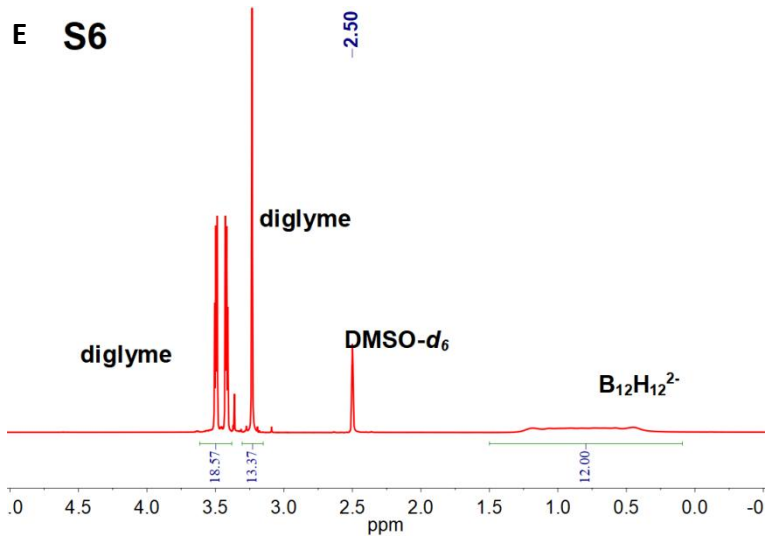
E
S6
2.50
diglyme
diglyme
DMSO-d_6
$B_{12}H_{12}^{2-}$
18.57
13.37
12.00
.0 4.5 4.0 3.5 3.0 2.5 2.0 1.5 1.0 0.5 0.0 -0
ppm

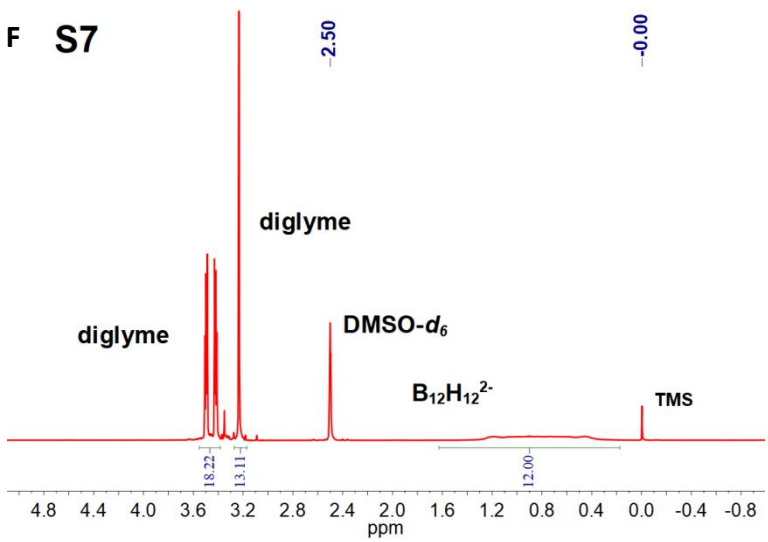
F
S7
2.50
0.00
diglyme
diglyme
DMSO-d_6
$B_{12}H_{12}^{2-}$
TMS
18.22
13.11
12.00
4.8 4.4 4.0 3.6 3.2 2.8 2.4 2.0 1.6 1.2 0.8 0.4 0.0 -0.4 -0.8
ppm

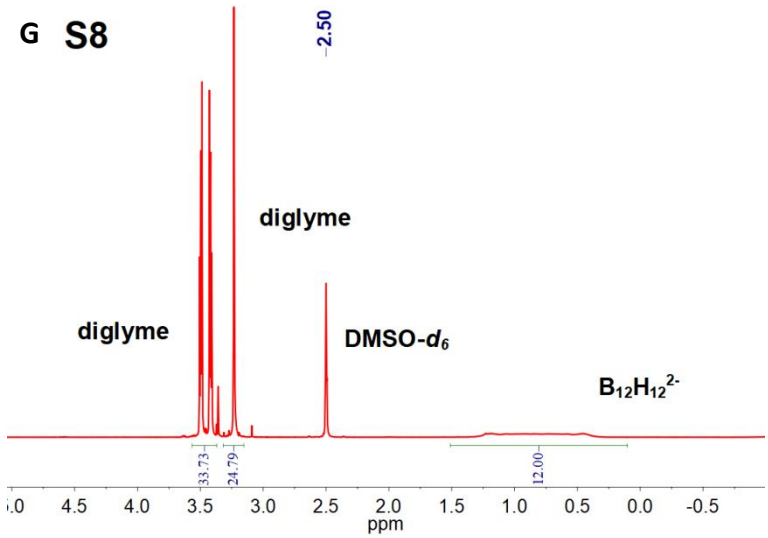

Supplementary Figure 11. Integrated ^{1}H NMR spectra of isolated $Li_2B_{12}H_{12}$ samples obtained in a Schlenk setup, according to the conditions described in Supplementary Table 3. Values indicated in blue correspond to the integration of the signals. The singlets at 3.31 ppm are due to residual water in the DMSO-d_6 used for dissolving the samples.

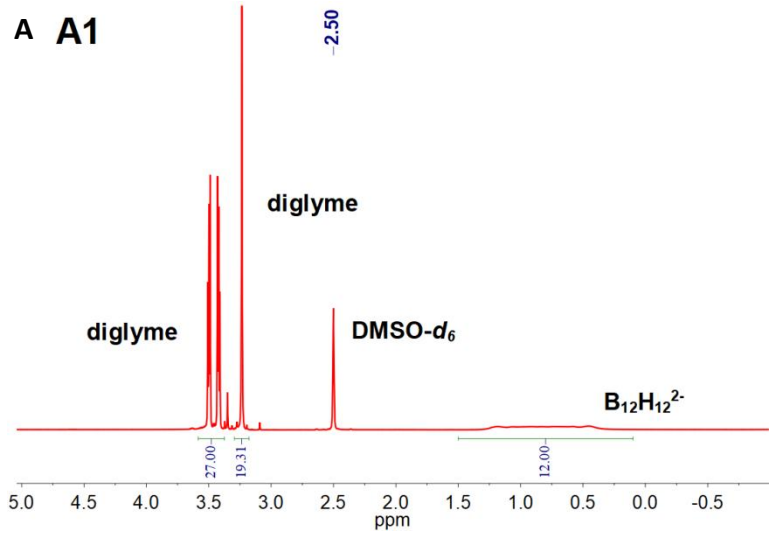
A
A1
2.50
diglyme
diglyme
DMSO-d_6
$B_{12}H_{12}^{2-}$
27.00
19.31
12.00
5.0 4.5 4.0 3.5 3.0 2.5 2.0 1.5 1.0 0.5 0.0 -0.5
ppm

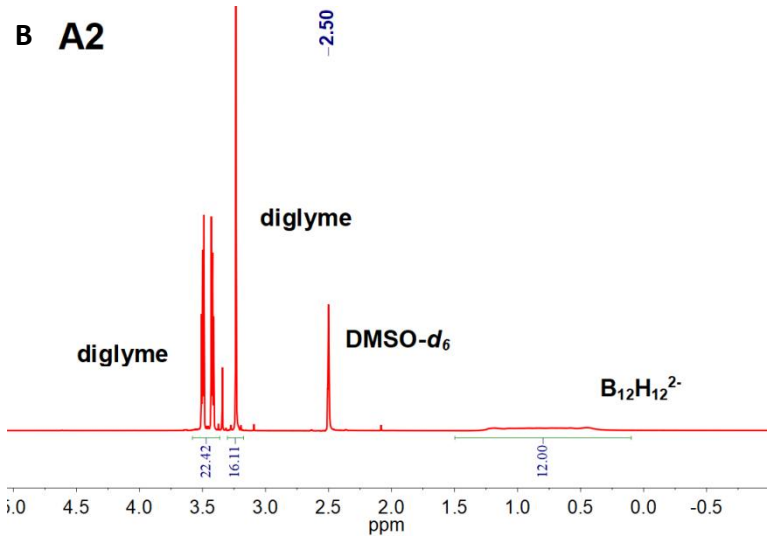
B
A2
2.50
diglyme
diglyme
DMSO-d_6
$B_{12}H_{12}^{2-}$
22.42
16.11
12.00
5.0 4.5 4.0 3.5 3.0 2.5 2.0 1.5 1.0 0.5 0.0 -0.5
ppm

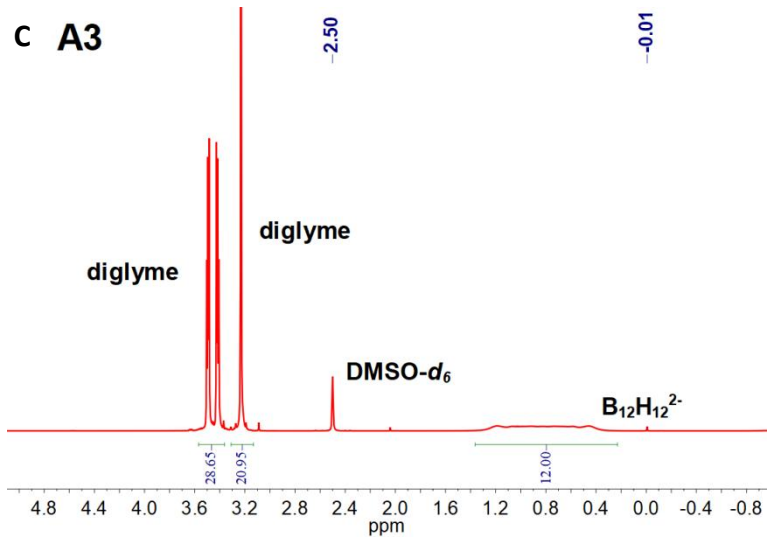
C
A3
2.50
0.01
diglyme
diglyme
DMSO-d_6
$B_{12}H_{12}^{2-}$
28.65
20.95
12.00
4.8 4.4 4.0 3.6 3.2 2.8 2.4 2.0 1.6 1.2 0.8 0.4 0.0 -0.4 -0.8
ppm

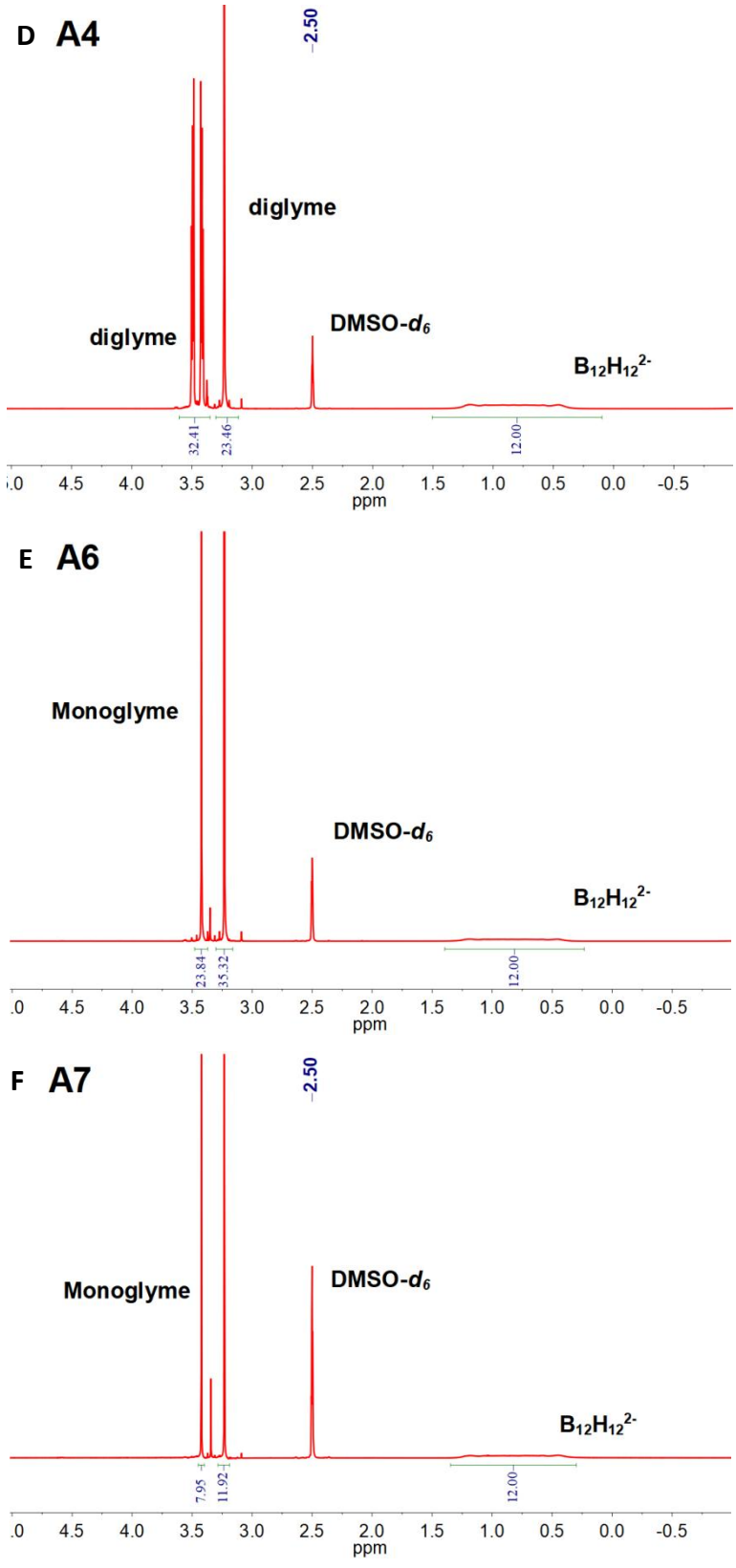

Supplementary Figure 12. Integrated ^{1}H NMR spectra of isolated $Li_2B_{12}H_{12}$ samples obtained in an autoclave, according to the conditions described in Supplementary Table 4. The singlets at 3.31 ppm are due to residual water in the DMSO-d_6 used for dissolving the samples.

6 Previous synthetic methods of $B_{12}H_{12}^{2-}$ salts

Supplementary Table 8. Summary of reported methods for the synthesis of $B_{12}H_{12}^{2-}$ salts.

Code	Reaction	Condition	Purity	Yields
1[3]	2-Iododecaborane+$N(C_2H_5)_3$	Refluxing benzene, 5 h	n/a	4 %
2[4]	$2NaBH_4 + 5B_2H_6 \rightarrow Na_2B_{12}H_{12} + 13H_2$ $2(C_2H_5)_3N{\cdot}BH_3 + 5B_2H_6 \rightarrow [(C_2H_5)_3NH]_2B_{12}H_{12} + 13H_2$	Ethers, 100-180°C	n/a	90 %
3[5]	$Mg(BH_4)_2 + 5B_2H_6 \rightarrow MgB_{12}H_{12} + 13H_2$	150°C, 24 h	22.3 mol %	n/a
4[6]	$2LiBH_4 + 5B_2H_6 \rightarrow Li_2B_{12}H_{12} + 13H_2$	150 °C, 10 bar H_2/B_2H_6	94 %	n/a
5[4]	$B_{10}H_{14} + Et_3NBH_3 \rightarrow B_{12}H_{12}^{2-}$	190 °C	n/a	92 %
6[7]	$B_{10}H_{14} + NaBH_4 \rightarrow Na_2B_{12}H_{12} + 3\ H_2$	Diglyme, 160 °C	n/a	91 %
7[8]	$2MH+1.2B_{10}H_{14} \rightarrow M_2B_{12}H_{12}+ 3.4H_2$ (M=Li, Na) $2MBH_4+B_{10}H_{14} \rightarrow M_2B_{12}H_{12}+5H_2$ (M=Li, Na, K)	Annealing 200−450 °C, 10-20 h	n/a	n/a
8[9]	$M(BH_4)_2 + B_{10}H_{14} \rightarrow MB_{12}H_{12} + 5H_2$ (M = Mg, Ca)	Annealing, 300°C Annealing, 380°C	n/a n/a	n/a
9[10]	$2LiBH_4 + B_{10}H_{14} \rightarrow Li_2B_{12}H_{12} + 5H_2$	135°C +180 °C 200°C, 15 h	93 % 62 %	n/a n/a
10[11]	MBH_4 (M = Na, K) + N,N-dipropylaniline borane	Diglyme, 120-140°C, 29-72 h	n/a	88 %
11[12]	$8(C_2H_5)_4N{\cdot}B_3H_8 \rightarrow [(C_2H_5)_4N]_2B_{12}H_{12}+[(C_2H_5)_4N]_2B_{10}H_{10}+4C_2H_6+16H_2+2\ (C_2H_5)_3N+2(C_2H_5)_3NBH_3$	Toluene, 185°C	n/a	n/a
12[13]	$3\ NaBH_4 + I_2 \rightarrow NaB_3H_8 + 2\ NaI + 2\ H_2$ $5\ NaB_3H_8 \rightarrow Na_2B_{12}H_{12} + 3\ NaBH_4 + 8\ H_2$	Diglyme, 100°C	n/a	50-60%
13[14]	$NaB_3H_8 \rightarrow Na_2B_{10}H_{10} + Na_2B_{12}H_{12}$	Ar, 150°C, 48 h	n/a	n/a
14[15]	$12NaBH_4+10R\text{-}Hal \rightarrow Na_2B_{12}H_{12}+10R\text{-}H+ 10NaCl+ 13H_2$	Ether	n/a	84%
15[1]	$2\ MBH_4 + 10\ (CH_3)_2S{\cdot}BH_3 \rightarrow M_2B_{12}H_{12} + 10\ (CH_3)_2S + 13\ H_2$ (M=Na, K)	Autoclave, diglyme	pure	85 % 84 %
16[16]	$KB_3H_8+KB_9H_{14}$ $KB_3H_8+KB_9H_{14}$ $NaB_{11}H_{14}+NaB_3H_8$	Diglyme, 120 °C, 36 h 1,4-dioxane, 90 °C Diglyme, 140 °C, 40 h	n/a	82% 0 80
This work	$2\ LiBH_4 + 10\ (CH_3)_2S{\cdot}BH_3 \rightarrow Li_2B_{12}H_{12} + 10\ (CH_3)_2S + 13\ H_2$	Autoclave, 120 °C, 48 h	pure	96 %
	$2\ NaBH_4 + 10\ (CH_3)_2S{\cdot}BH_3 \rightarrow Na_2B_{12}H_{12} + 10\ (CH_3)_2S + 13\ H_2$	160°C, refluxing diglyme, 24 h	pure	92 %
	$2\ KBH_4 + 10\ (CH_3)_2S{\cdot}BH_3 \rightarrow K_2B_{12}H_{12} + 10\ (CH_3)_2S + 13\ H_2$	160°C, refluxing diglyme, 24 h	90	88 %

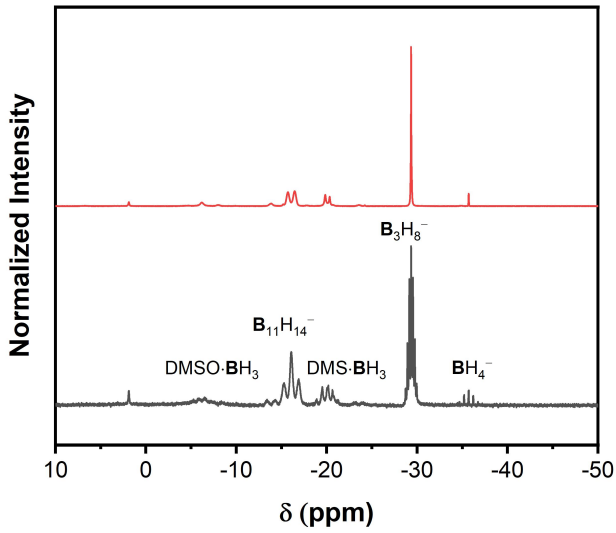

Supplementary Figure 13. Proton-coupled and decoupled ^{11}B NMR spectra of filtrates obtained upon reaction of 5 mmol $LiBH_4$ with 5 equiv (10% excess) of DMS·BH_3 for 24 hours at 120°C in an autoclave in diglyme.

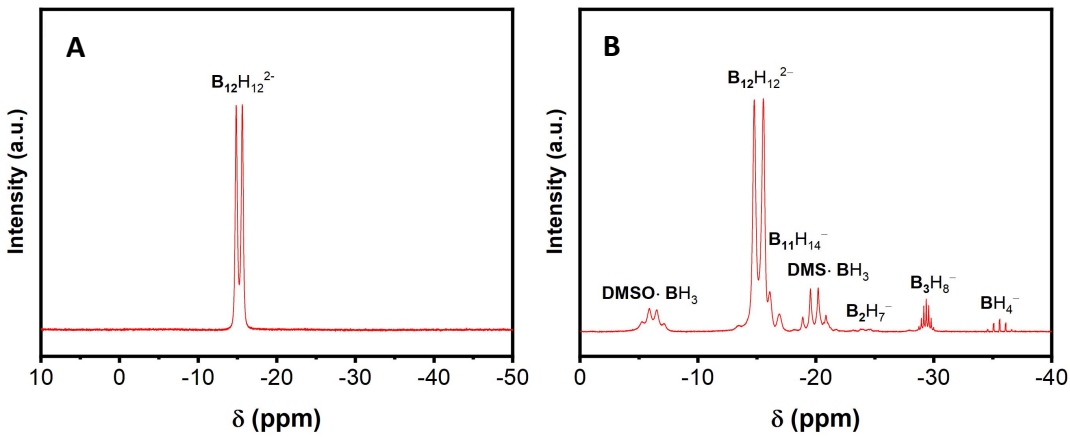

Supplementary Figure 14. Proton-coupled ^{11}B NMR spectra of (A) solid precipitate and (B) filtrate (10 mmol $LiBH_4$, autoclave, 24 h). The particles of $Li_2B_{12}H_{12}$ that remained suspended in the filtrate were fully dissolved by addition of DMSO-d_6 prior to analysis.

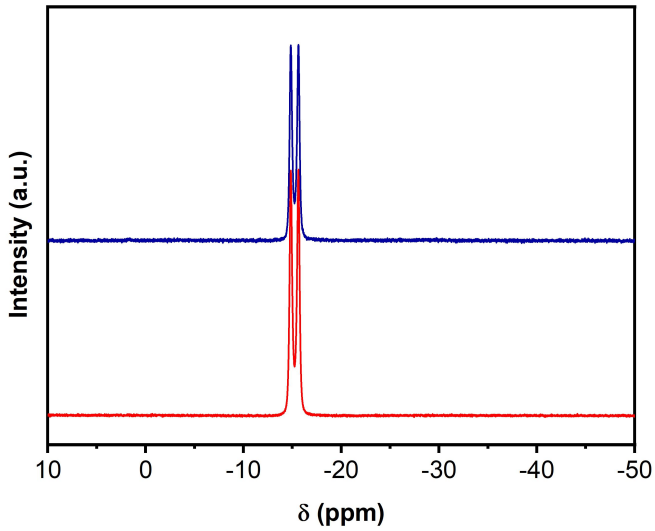

Supplementary Figure 15. Proton-coupled ^{11}B NMR spectra of two batches of solid precipitates obtained by reaction of 10 mmol $LiBH_4$ with 55 mmol (10% excess) of $DMS{\cdot}BH_3$ for 24 hours at 120°C in an autoclave (red = first batch, same spectrum as the one represented in Figure 2; blue = second batch).

7 Thermal behavior of diglyme solvated $Li_2B_{12}H_{12}$

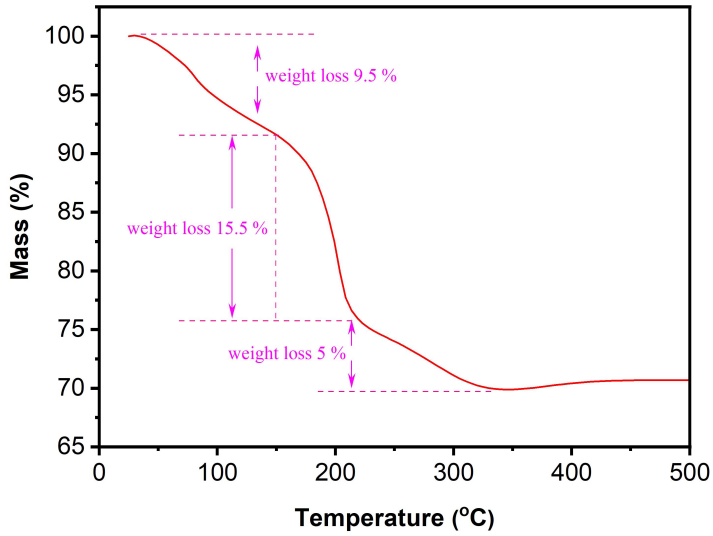

Supplementary Figure 16. TGA of as-synthesized $Li_2B_{12}H_{12}$.n diglyme (sample S6).

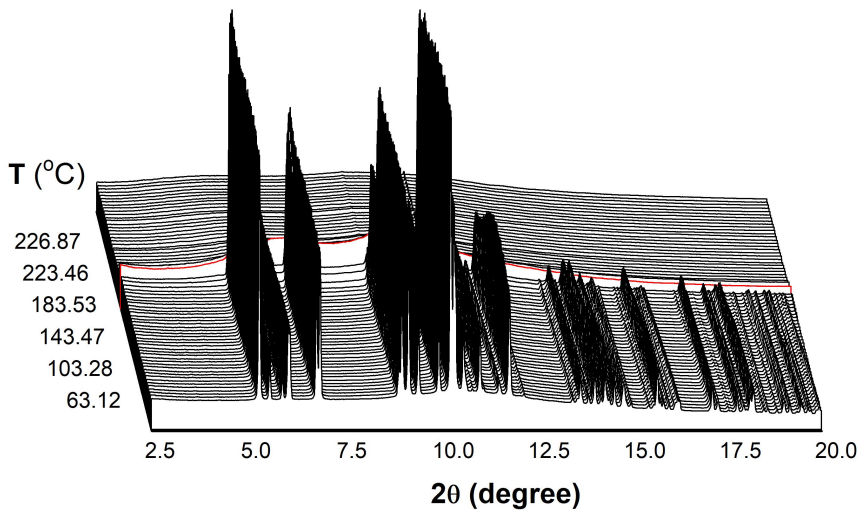

Supplementary Figure 17. In situ synchrotron radiation powder X-ray diffraction (SR-PXRD) data of $Li_2B_{12}H_{12}$·2 diglyme. Heating rate = 10 °C/min (λ = 0.77509 Å).

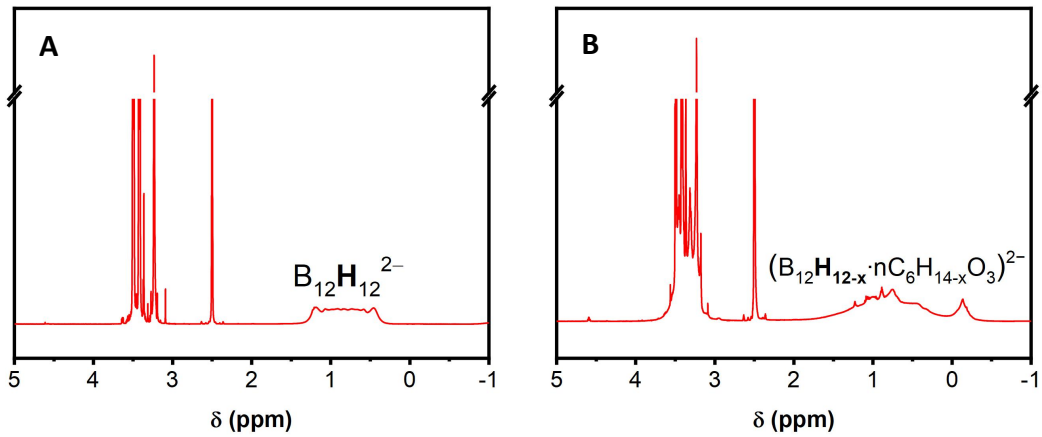

Supplementary Figure 18. ^{1}H NMR spectra of diglyme solvated $Li_2B_{12}H_{12}$ (A) before and (B) after heat treatment at 170 °C under vacuum. The characteristic multiplet of $B_{12}H_{12}^{2-}$ (1.6 – 0 ppm) disappears upon thermal treatment.

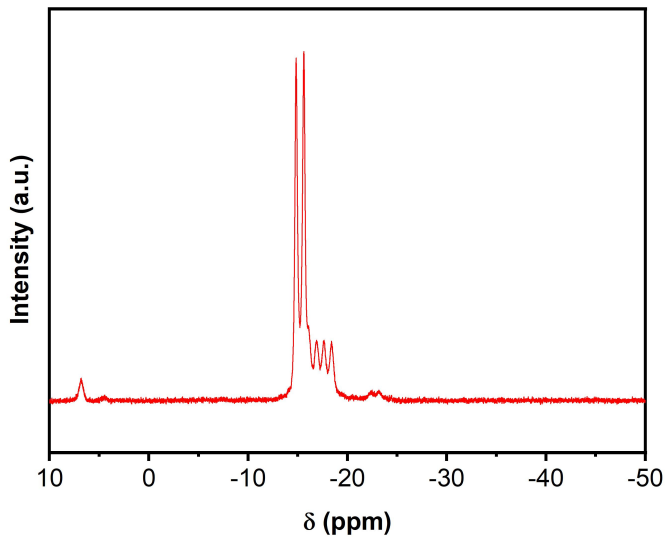

Supplementary Figure 19. Proton-coupled ^{11}B NMR spectrum of $Li_2B_{12}H_{12}{\cdot}n$ diglyme upon heating at 180 °C under air for 5 minutes.

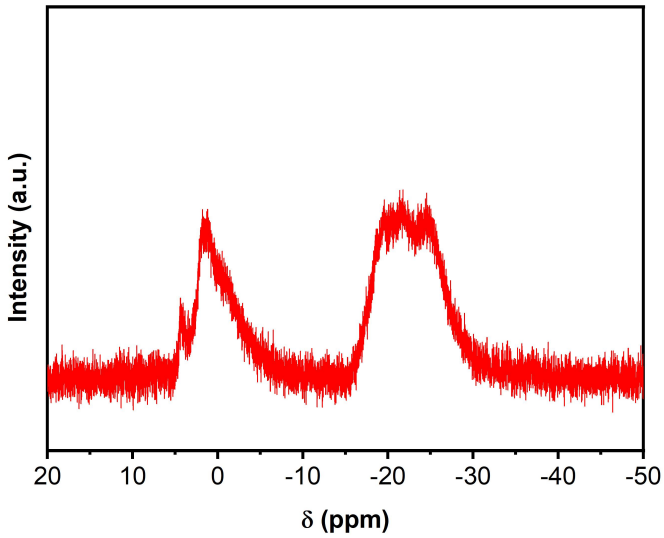

Supplementary Figure 20. Proton-coupled ^{11}B NMR spectrum of $Li_2B_{12}H_{12}$·n diglyme upon heating at 180 °C under air for 12 h.

8 Removal of DMSO from $Li_2B_{12}H_{12}$·n DMSO

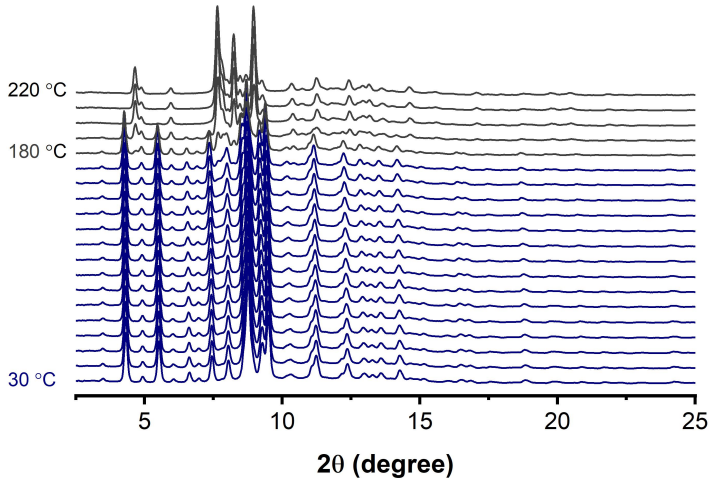

Supplementary Figure 21. Vacuum in situ PXRD patterns of the DMSO-rich solvate of $Li_2B_{12}H_{12}$ obtained upon preliminary drying at 100 °C under vacuum (λ = 0.71073 Å).

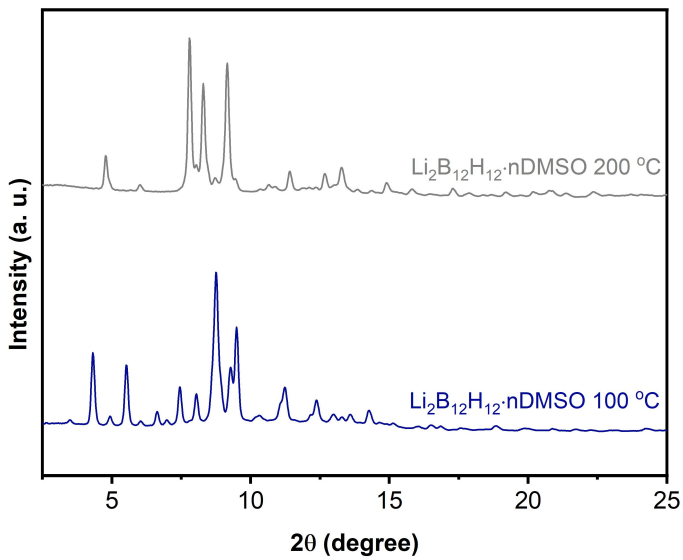

Supplementary Figure 22. PXRD patterns of the DMSO-rich (dried at 100 °C under vacuum) and DMSO-poor (dried at 200 °C under argon flow) solvates of $Li_2B_{12}H_{12}$ (λ = 0.71073 Å).

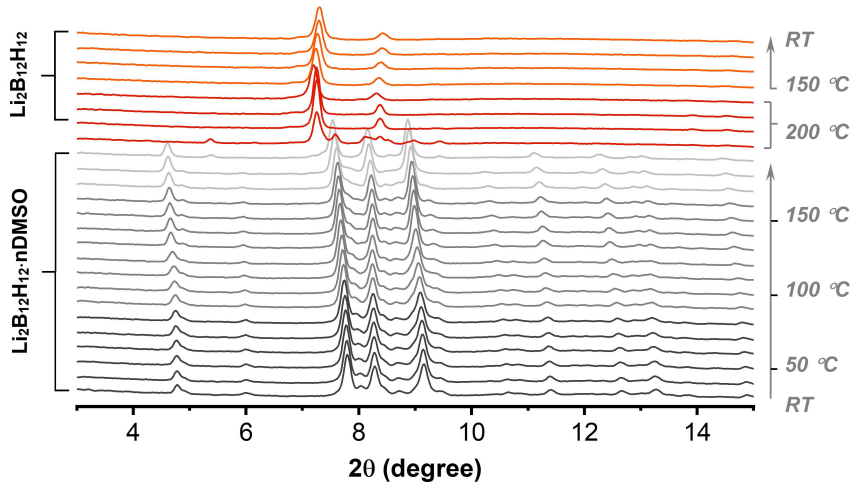

Supplementary Figure 23. Vacuum in situ PXRD patterns of the DMSO-poor solvate of $Li_2B_{12}H_{12}$ obtained upon preliminary drying at 200 °C under argon flow (λ = 0.71073 Å).

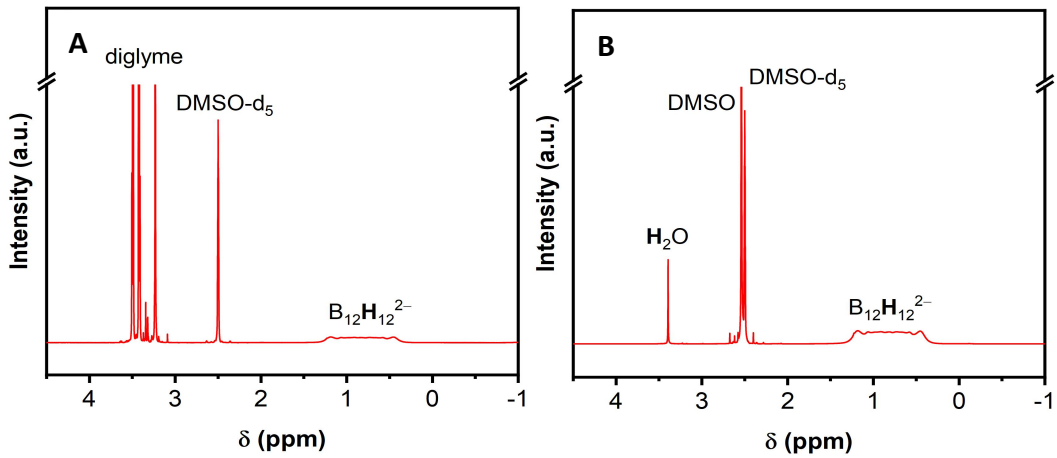

Supplementary Figure 24. ^{1}H NMR spectra of (A) $Li_2B_{12}H_{12}$·n diglyme and (B) $Li_2B_{12}H_{12}$· n DMSO.

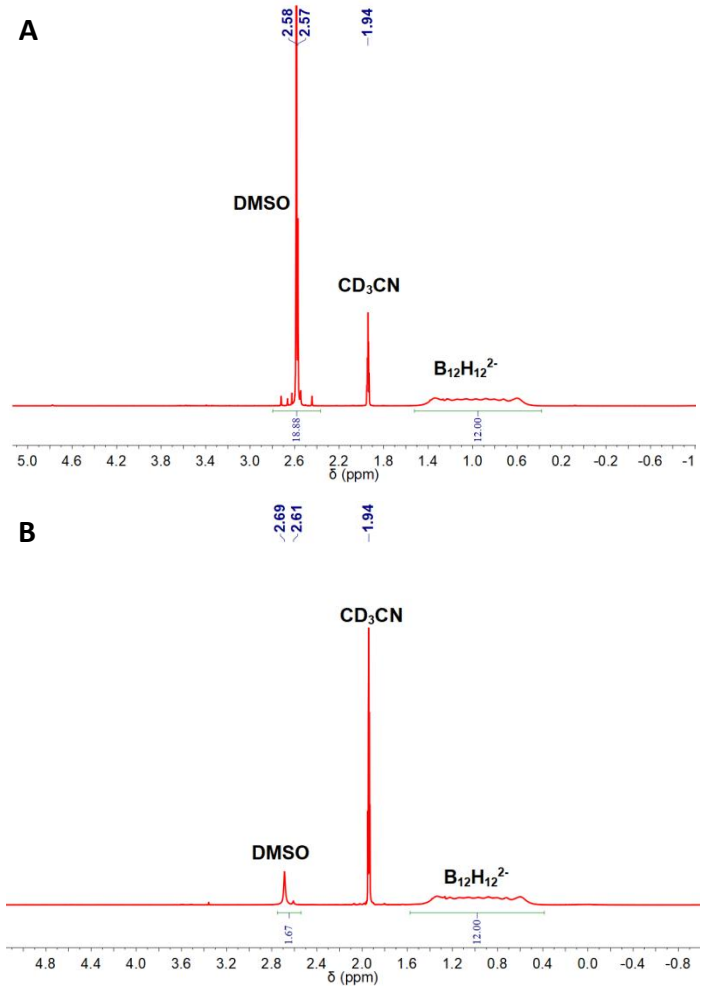

Supplementary Figure 25. ^{1}H NMR spectra of DMSO solvated $Li_2B_{12}H_{12}$ (A) before and (B) after heat treatment at 200 °C under vacuum for 12h. Samples were dissolved in CD_3CN-d_3.

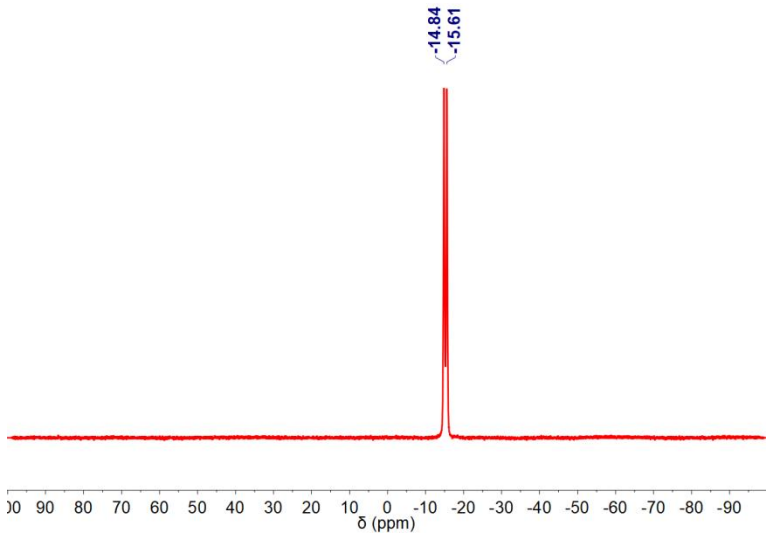

Supplementary Figure 26. ^{11}B NMR spectrum of $Li_2B_{12}H_{12}$·n DMSO after heat treatment at 200 °C under vacuum for 12h.

Note: The in situ PXRD experiments on $Li_2B_{12}H_{12}$·n DMSO were first performed with the solvated form of $Li_2B_{12}H_{12}$·n DMSO obtained after preliminary treatment at 100 °C under vacuum. However, the high boiling point of DMSO caused it to condense in the colder parts of the capillary, resulting in a DMSO-rich atmosphere that could affect the measurements. To address this issue, some sample was preliminary dried at 200 °C under argon to obtain a DMSO-poor phase. An in situ PXRD measurement was then performed on this phase, enabling to observe the desolvation into anhydrous $Li_2B_{12}H_{12}$.

Note on the use of alternative methods to remove diglyme from $Li_2B_{12}H_{12}$

It is worth noting that lighter solvents were investigated for the removal of diglyme. CH_2Cl_2 was able to lower the amount of free diglyme in the final product and to facilitate the recrystallization of $Li_2B_{12}H_{12}$.2 diglyme, but it also resulted in sample loss. Toluene was only able to partially lower the amount of free diglyme. The use of H_2O was not as effective to remove diglyme. Although H_2O has a higher polarity than diglyme and is able to lower the amount of coordinated diglyme, its lower boiling point and vapor pressure made it difficult to remove the latter completely from the product. The use of H_2O combined with rotary evaporation is more effective in lowering the amount of diglyme, although it requires a much longer duration for complete solvent removal. Organic solvents, such as ethyl acetate or Et_2O, can be used to extract the diglyme from the aqueous solution of diglyme solvated $Li_2B_{12}H_{12}$ before evaporation, but such a process requires more steps and does not enable to remove the totality of the diglyme. A system enabling to achieve higher vacuum for solvent removal by using a turbomolecular pump was also investigated for the desolvation of $Li_2B_{12}H_{12}$·n diglyme, but was ineffective.

As a general trend, the diglyme-solvated form of $Li_2B_{12}H_{12}$ exhibits relatively low solubility in lighter ethers such as Et_2O, THF, and DME, making it challenging to use those solvents for diglyme substitution. The choice of solvent for the removal of coordinated diglyme from the solvated $Li_2B_{12}H_{12}$ must thus be carefully considered to ensure maximum efficiency.

9 Removal of monoglyme from $Li_2B_{12}H_{12}$·n $C_4H_{10}O_2$

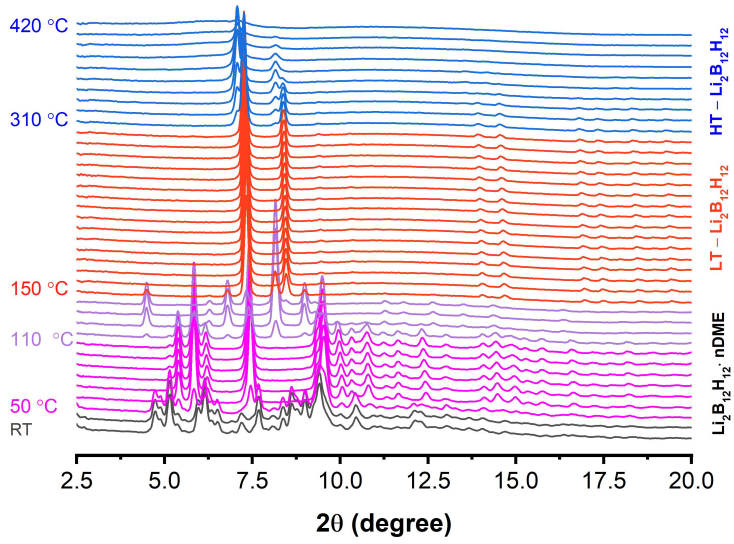

Supplementary Figure 27. In situ powder X-ray diffraction data of a monoglyme-rich $Li_2B_{12}H_{12}$·n DME sample (λ = 0.71073 Å).

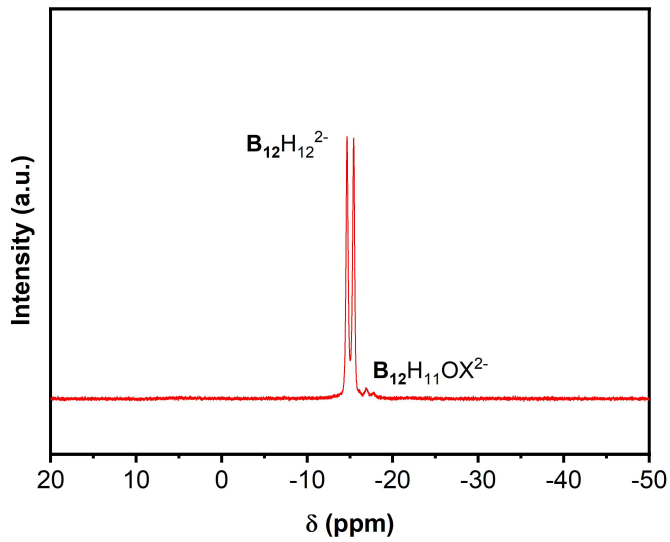

Supplementary Figure 28. Proton-coupled ^{11}B NMR spectrum of DME solvated $Li_2B_{12}H_{12}$ after drying at 180°C for 12 h under vacuum. The sample was dissolved in CD_3CN-d_3 for the measurement.

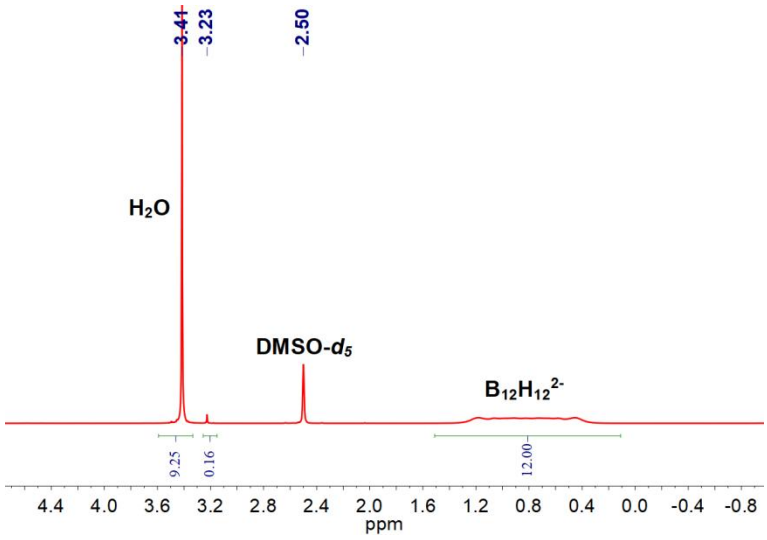

Supplementary Figure 29. ^{1}H NMR spectrum of H_2O substituted DME solvated $Li_2B_{12}H_{12}$ after addition of H_2O (10 ml for 1 g of sample) and heat treatment at 40 °C under vacuum.

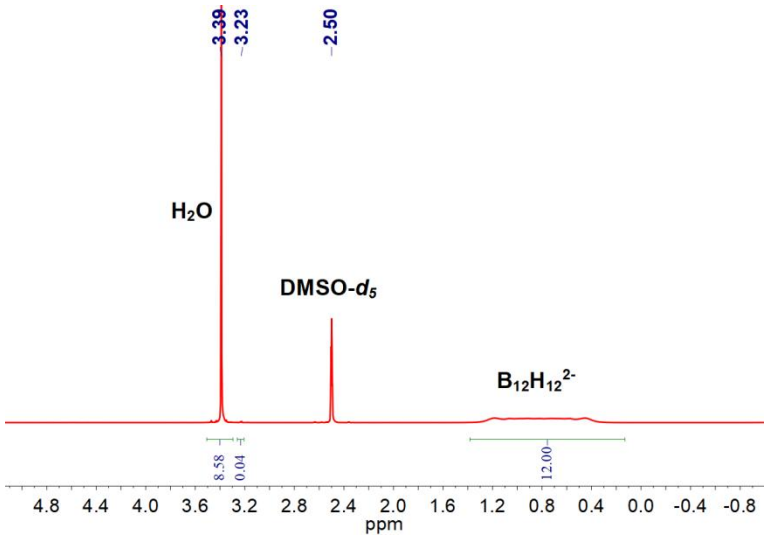

Supplementary Figure 30. ^{1}H NMR spectrum of H_2O substituted DME solvated $Li_2B_{12}H_{12}$ after 3 subsequent treatments with H_2O (10 ml each time, for 1 gram of sample) and heat treatment at 40 °C under vacuum until dryness.

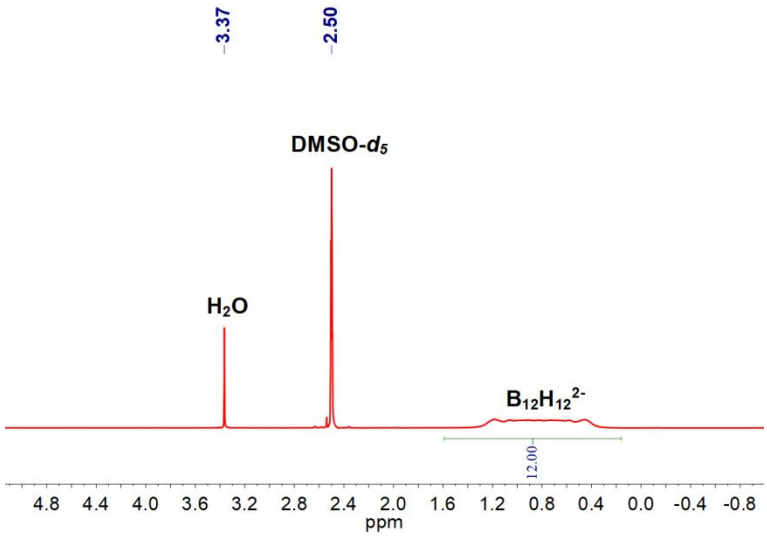

Supplementary Figure 31. ^{1}H NMR spectrum of desolvated $Li_2B_{12}H_{12}$·n H_2O after heat treatment at 200 °C under vacuum for 12h. The observed signal of H_2O (HDO) results from traces of moisture in the used DMSO-d_6.

Residual DME present in the samples obtained after heat treatment of $Li_2B_{12}H_{12}$·n DME can be observed on the FTIR spectra. Complete removal of DME at high temperature (180 °C) is accompanied by the formation of partially dehydrogenated $B_{12}H_{12-x}$· n $C_6H_{14-x}O_3^{2-}$, as shown in Supplementary Figure 28. The ^{1}H NMR spectrum (Supplementary Figure 30) indicates that DME can be completely removed by treating the sample with H_2O, and H_2O can subsequently easily be removed by thermal treatment. By combining the results of FTIR (Figure 3F) and ^{1}H NMR analyses (Supplementary Figures 29-31) of desolvated $Li_2B_{12}H_{12}$·n H_2O, it can be concluded that $Li_2B_{12}H_{12}$ is completely anhydrous after the thermal treatment, as the vibration bonds for H_2O disappear from the FTIR spectrum.

10 Synthesis of $Na_2B_{12}H_{12}$ and $K_2B_{12}H_{12}$ in Schlenk flask under reflux

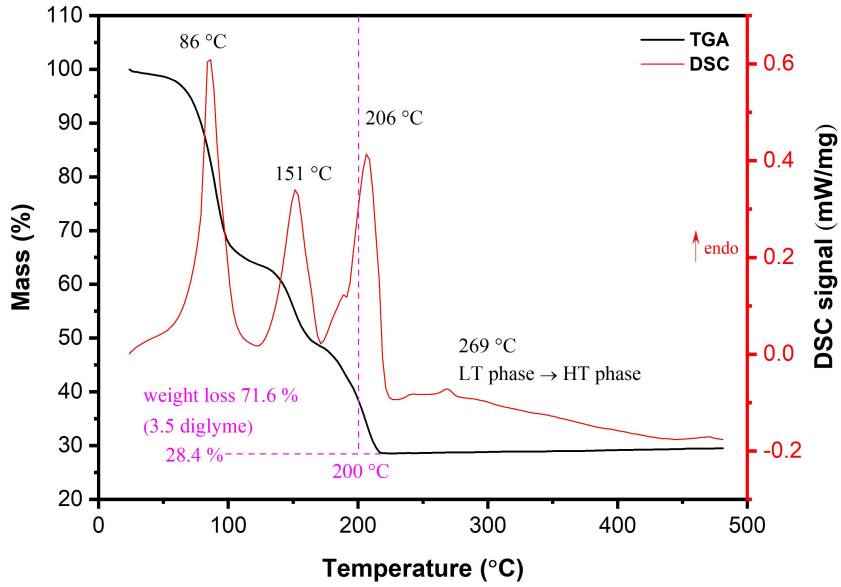

Supplementary Figure 32. TGA-DSC analysis of as-synthesized $Na_2B_{12}H_{12}$.n diglyme, after initial drying under vacuum at room temperature.

Note: A single crystal of $Na_2B_{12}H_{12}$·4 diglyme was isolated from the reaction mixture upon reaction between $NaBH_4$ and DMS·BH_3. Initial washing and drying at room temperature resulted in the partial desolvation from $Na_2B_{12}H_{12}$·4 diglyme to $Na_2B_{12}H_{12}$·7/2 diglyme. TGA/DSC revealed that the loss of diglyme from $Na_2B_{12}H_{12}$·3.53 diglyme occurs in three distinct steps: the first one resulted in the formation of $Na_2B_{12}H_{12}$·5/3 diglyme, in the second step, about 2/3 molecules of diglyme are removed, resulting in $Na_2B_{12}H_{12}$·diglyme, and in the final stage, all diglyme molecules are removed, leading to anhydrous $Na_2B_{12}H_{12}$. Those three solvent removal steps are accompanied by intense endothermic peaks on the DSC curve at around 86°C, 151°C and 206°C, respectively. These results indicate that diglyme solvated metal dodecaborates are metastable compounds which lose diglyme molecules in a stepwise manner upon heating.

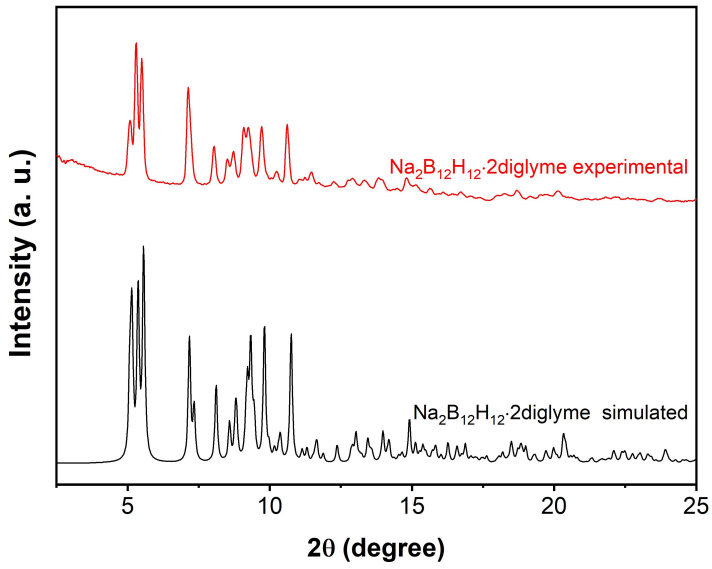

Supplementary Figure 33. Experimental PXRD pattern of as-synthesized diglyme solvated $Na_2B_{12}H_{12}$ sample upon initial drying at 80 °C under vacuum, and simulated pattern from the structure solved from a single crystal of $Na_2B_{12}H_{12}$·2 diglyme (λ = 0.71073 Å).

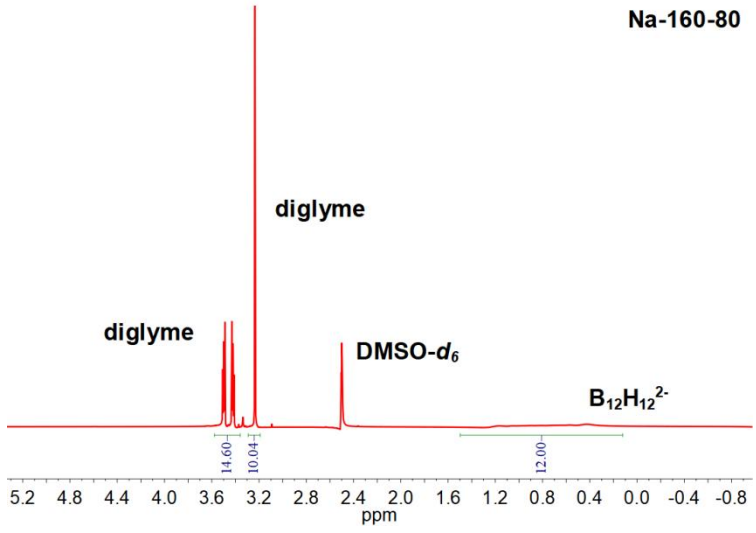

Supplementary Figure 34. Integrated ^1H NMR spectrum of diglyme solvated $Na_2B_{12}H_{12}$ upon initial drying at 80 °C under vacuum. The composition of the sample was determined as $Na_2B_{12}H_{12}$·1.76 diglyme.

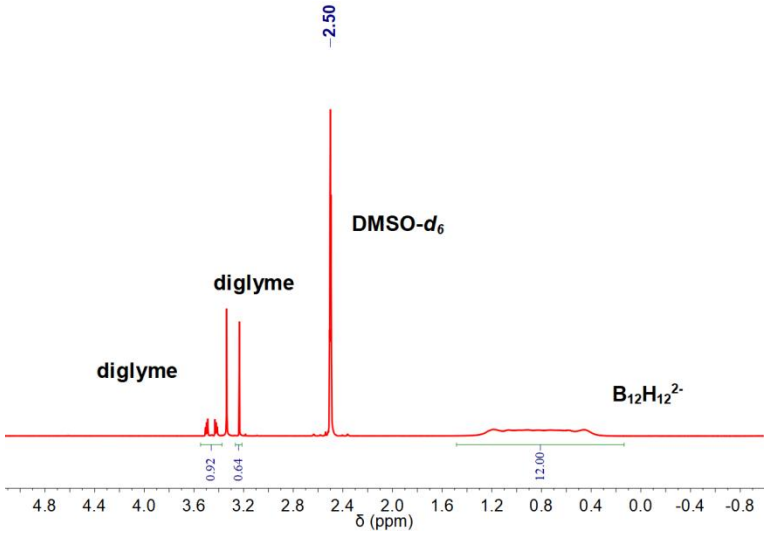

Supplementary Figure 35. Integrated ^{1}H NMR spectrum of diglyme solvated $Na_2B_{12}H_{12}$ upon drying at 200 °C for 2h under vacuum.

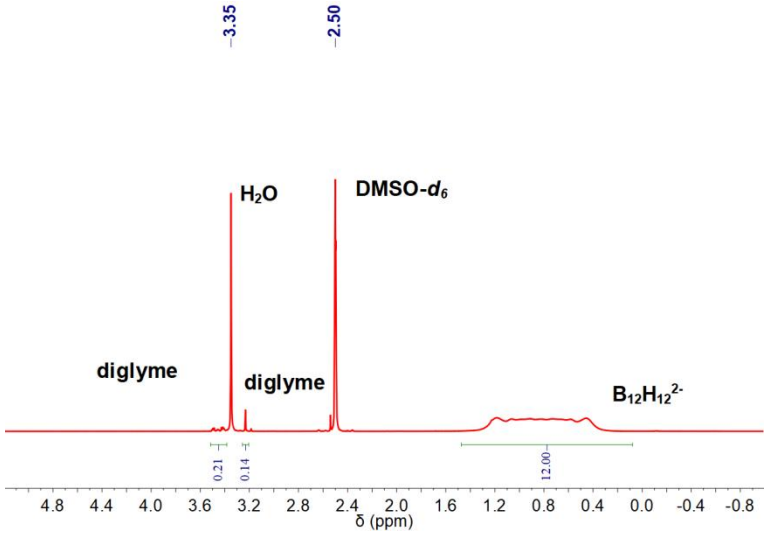

Supplementary Figure 36. Integrated ^{1}H NMR spectrum of diglyme solvated $Na_2B_{12}H_{12}$ upon addition of H_2O (10 ml for 1 g of sample) and drying at 200 °C for 2h under vacuum.

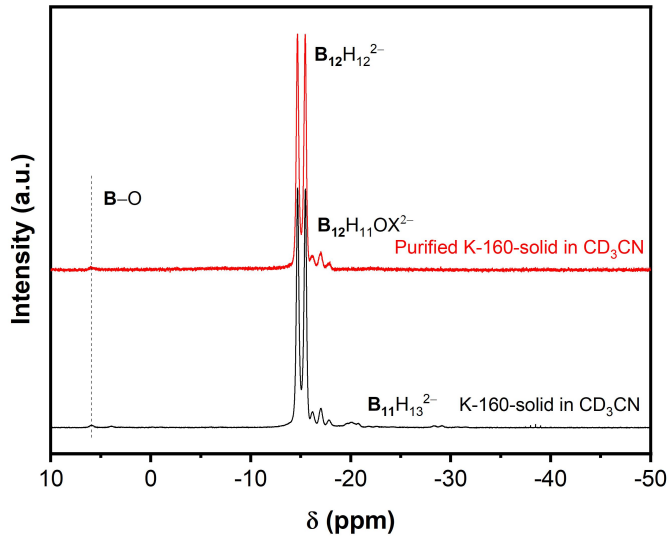

Supplementary Figure 37. Proton-coupled ^{11}B NMR spectra of product obtained by reaction between KBH_4 and 5 equiv (10% excess) of $DMS{\cdot}BH_3$ before (black) and after (red) purification with H_2O.

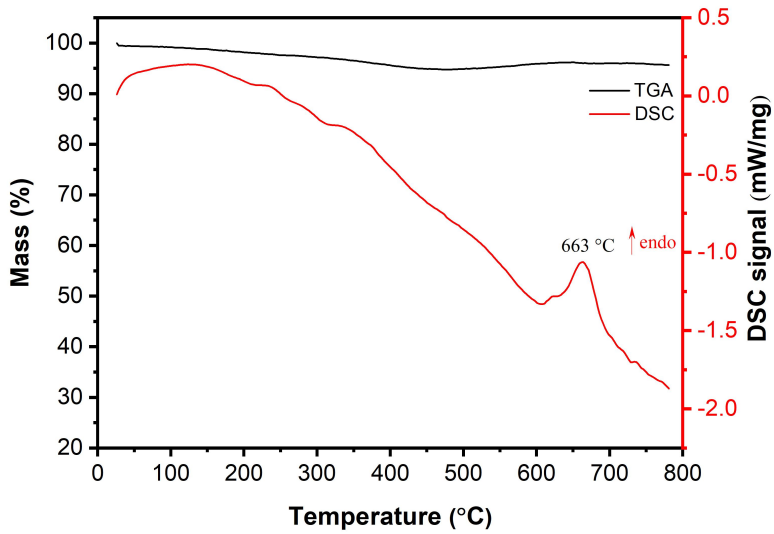

Supplementary Figure 38. TGA-DSC of purified $K_2B_{12}H_{12}$ after initial drying at 150 °C.

The TGA-DSC of $K_2B_{12}H_{12}$ reveals an evident endothermic peak at 663 °C, typical of the decomposition of $K_2B_{12}H_{12}$ and the polymerization of $K_2B_{12}H_{12}$ to $(K_2B_{12}H_n)_m$. However, it is worth noting that a phase transition of $K_2B_{12}H_{12}$ is expected to occur at a lower temperature based on a previous report. [9,17] $K_2B_{12}H_{12}$ can be purified according to a procedure reported in our earlier work, consisting in removing $B_{11}H_{13}^{2-}$ and BH_4^- through treatment with hot water. This leads to a solid residue containing $B_{12}H_{12}^{2-}$ and

$B_{12}H_{12-x}\cdot$ n $C_6H_{14-x}O_3^{2-}$ (closomers), which can be separated by extraction with a less polar solvent like alcohols for instance. To minimize the formation of $B_{12}H_{12-x}\cdot$ n $C_6H_{14-x}O_3^{2-}$ during the synthesis of $K_2B_{12}H_{12}$, milling of KBH_4 to smaller-sized crystallites prior to use for the synthesis has been proven to be advantageous. [1] It should be noted that when KBH_4 is used for the synthesis of higher boranes, traces of KBH_4 may still be detected in the final products, due to its low solubility in most ethereal solvents.

11 Synthesis in toluene

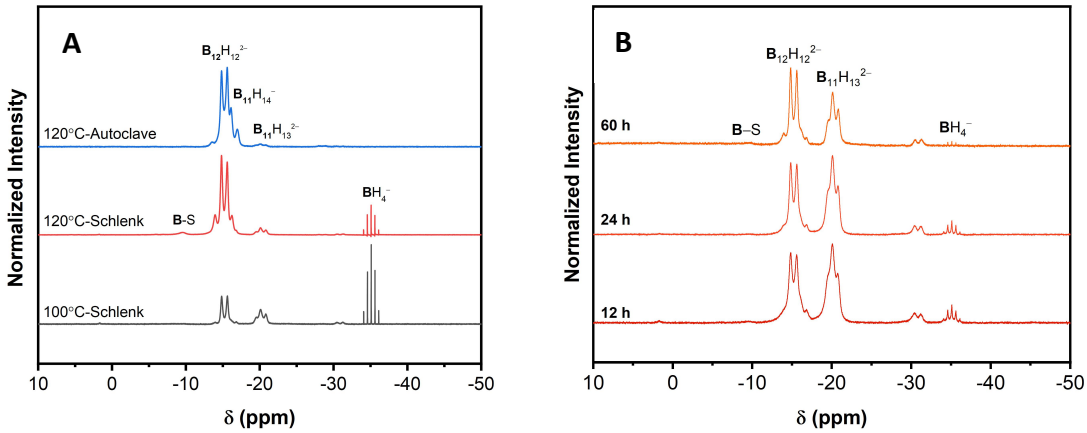

Supplementary Figure 39. Proton-coupled ^{11}B NMR spectra of (A) solid compounds obtained from 5 mmol $LiBH_4$ + 27.5 mmol $DMS{\cdot}BH_3$ in 20 ml toluene at 100°C and 120°C for 24 hours, in a Schlenk flask or autoclave and (B) of 5 mmol ball-milled $LiBH_4$ with 27.5 mmol of $DMS{\cdot}BH_3$ after various reaction times at 120 °C in a Schlenk flask.

The reactions were also attempted in toluene, a non-coordinating solvent, with the aim of directly obtaining unsolvated $Li_2B_{12}H_{12}$. [8,10,18] The NMR spectra (Supplementary Figure 39A and Supplementary Figures 40-41) of the solubilized solid sample obtained from reaction in a Schlenk setup shows the presence of the desired $B_{12}H_{12}^{2-}$ along with BH_4^-, $B_{11}H_{14}^-$, $B_{11}H_{13}^{2-}$ and $B_{12}H_{11}S(CH_3)^-$ in the final solid. The formation of $B_{12}H_{11}S(CH_3)^-$ can be attributed to the self-condensation of $DMS{\cdot}BH_3$. [19] The diffraction patterns (Supplementary Figures 42-44) of the sample obtained by running the reaction at 100 °C however indicates the presence of $Li_2B_{12}H_{12}$ as only crystalline phase. A higher temperature of 120 °C leads to a solid showing diffraction peak of impurity phases along the desired phase. In contrast, experiments performed in an autoclave enabled the complete conversion of BH_4^- into $B_{11}H_{14}^-$, $B_{11}H_{13}^{2-}$ and $B_{12}H_{12}^{2-}$. We also ball-milled $LiBH_4$ prior to the synthesis in toluene in the Schlenk setup to further improve the synthesis, as this reactant exhibits insolubility in this solvent. ^{11}B NMR spectra (Supplementary Figure 39B and Supplementary Figures 45-48) shows that this led to the presence of only BH_4^- and $B_{11}H_{13}^{2-}$ along with $B_{12}H_{12}^{2-}$ in the final solid. A considerable amount of $B_{11}H_{13}^{2-}$ is obtained after 24 hours and a longer reaction time is required for its conversion into $B_{12}H_{12}^{2-}$. As we observed that $B_{11}H_{13}^{2-}$ is insoluble in THF-d_8 (Supplementary Figure 49), its isolation was attempted by

washing the synthesized sample with excess THF (Supplementary Figure 50). However, we did not succeed in purifying the desired product, as $B_{12}H_{12}^{2-}$ and BH_4^- were still present after this washing procedure; completely isolating unsolvated $B_{11}H_{13}^{2-}$ without other boron-hydrogen compounds is challenging. It is noteworthy that similar reactions performed with ball-milled $NaBH_4$ instead of $LiBH_4$ resulted in the formation of $NaB_{12}H_{11}S(CH_3)_2$ as the main product (Supplementary Figures 51-52).

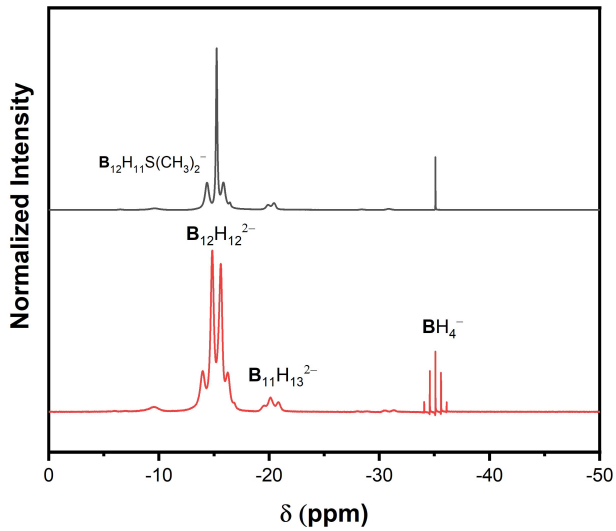

Supplementary Figure 40. Proton-coupled (red) and proton-decoupled (black) ^{11}B NMR spectra of solid samples obtained by reaction of 5 mmol $LiBH_4$ with 27.5 mmol (10% excess) of $DMS{\cdot}BH_3$ in 20 ml toluene for 24 hours at 120°C. The sample was washed with 3x5 ml diglyme. The absence of $B_{11}H_{13}^{2-}$ signals after the diglyme washing is explained by the solubility of this species in glymes.

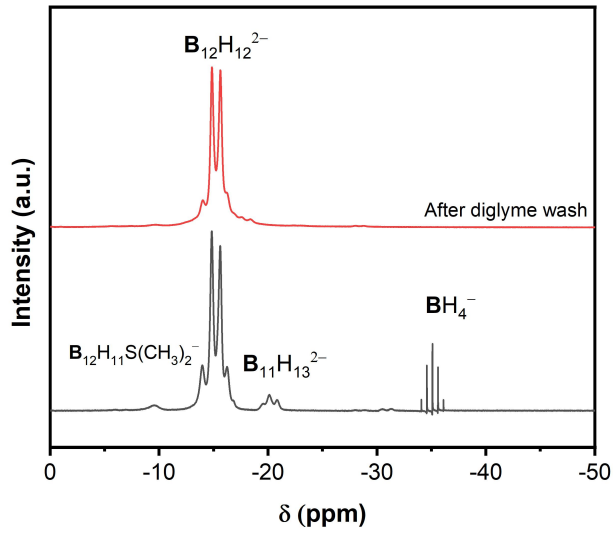

Supplementary Figure 41. Proton-coupled ^{11}B NMR spectra of solid samples obtained by reaction of 5 mmol $LiBH_4$ with 27.5 mmol (10% excess) of $DMS{\cdot}BH_3$ in 20 ml toluene for 24 hours at 120°C before (black) and after (red) diglyme washing.

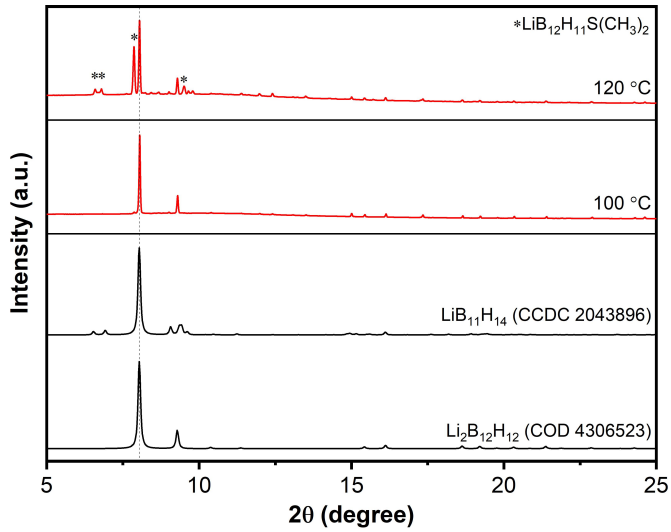

Supplementary Figure 42. Synchrotron radiation powder X-ray diffraction (SR-PXRD) patterns of solid samples obtained by reaction of 5 mmol ball-milled $LiBH_4$ with 27.5 mmol (10% excess) of $DMS{\cdot}BH_3$ in 20 ml toluene for 24 hours at 100°C or 120°C (λ = 0.77509 Å).

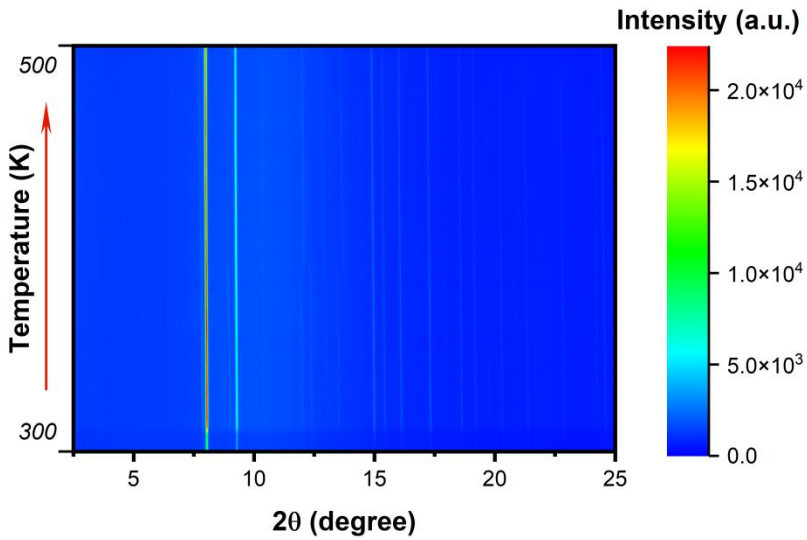

Supplementary Figure 43. In situ variable temperature synchrotron radiation powder X-ray diffraction (SR-PXRD) data of solid samples obtained by reaction of 5 mmol ball-milled $LiBH_4$ with 27.5 mmol (10% excess) of $DMS{\cdot}BH_3$ in 20 ml toluene for 24 hours at 100°C. Heating rate = 10 °C/min (λ = 0.77509 Å).

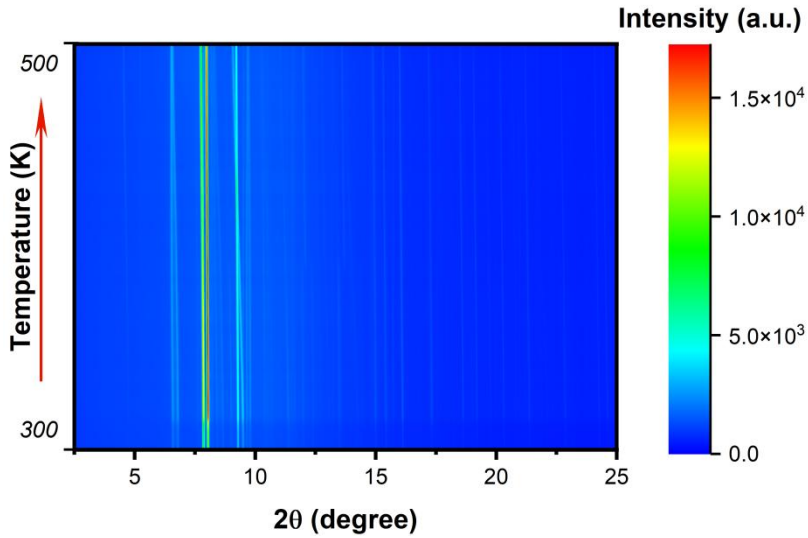

Supplementary Figure 44. In situ variable temperature synchrotron radiation powder X-ray diffraction (SR-PXRD) data of solid samples obtained by reaction of 5 mmol ball-milled $LiBH_4$ with 27.5 mmol (10% excess) of $DMS{\cdot}BH_3$ in 20 ml toluene for 24 hours at 120°C. Heating rate = 10 °C/min (λ = 0.77509 Å).

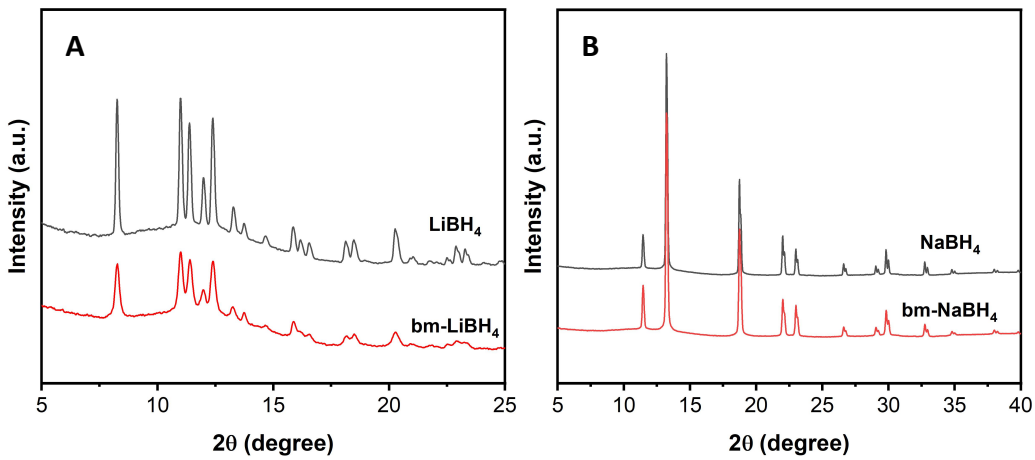

Supplementary Figure 45. PXRD patterns of commercial and ball-milled (A) $LiBH_4$ and (B) $NaBH_4$.

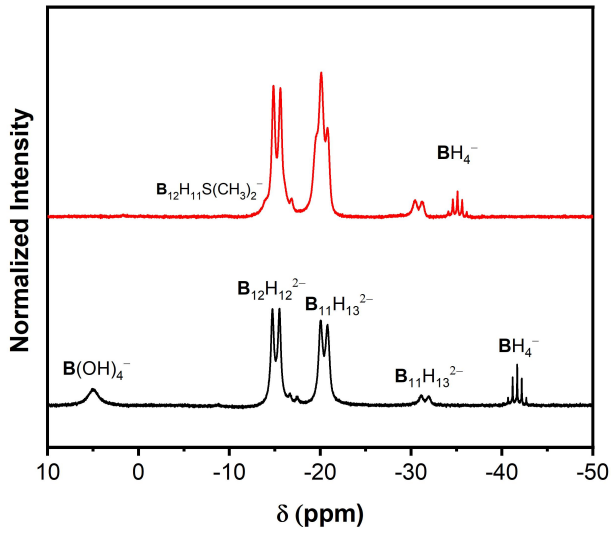

Supplementary Figure 46. Proton-coupled ^{11}B NMR spectra in D_2O (black) and DMSO-d_6 (red) of solid samples obtained by reaction of 5 mmol ball-milled $LiBH_4$ with 5 equiv (10 % excess) of DMS·BH_3 for 24 hours at 120°C in toluene in a Schlenk setup.

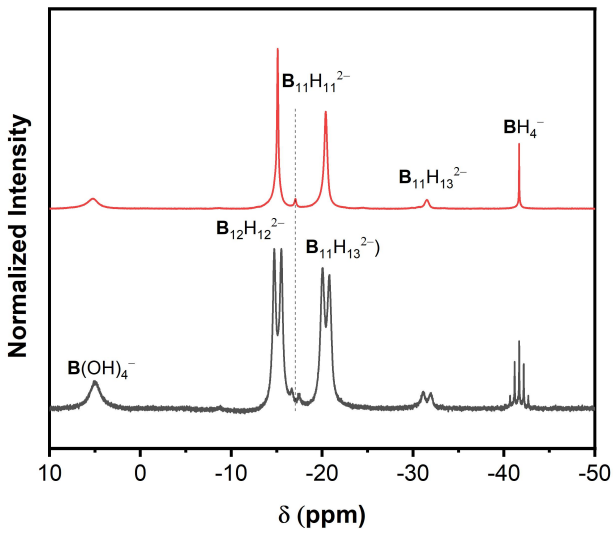

Supplementary Figure 47. Proton-coupled (black) and decoupled (red) ^{11}B NMR spectra of solid samples obtained by reaction of 5 mmol ball-milled $LiBH_4$ with 5 equiv (10 % excess) of DMS·BH_3 for 24 hours at 120°C in toluene in a Schlenk setup. Samples were dissolved in D_2O.

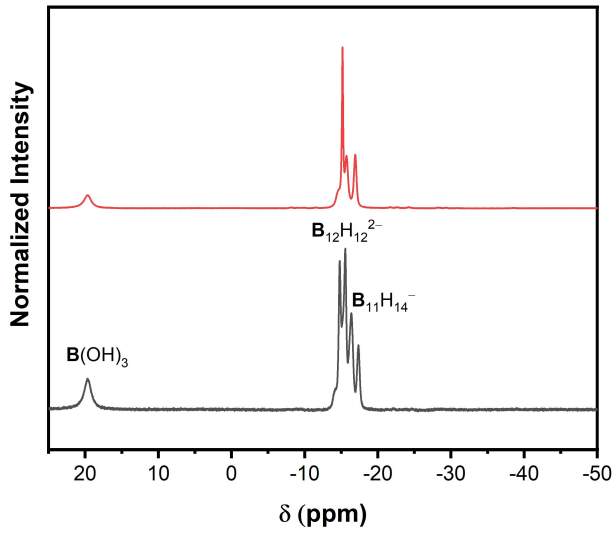

Supplementary Figure 48. Proton-coupled (black) and decoupled (red) ^{11}B NMR spectra of sample obtained by reaction of 5 mmol ball-milled $LiBH_4$ with 5 equiv (10 % excess) of $DMS{\cdot}BH_3$ for 24 hours at 120°C in toluene in a Schlenk setup. Prior to the measurement, 3M HCl was added dropwise to the solution until no further formation of bubbles was observed, to completely convert the $B_{11}H_{13}^{2-}$ anion into $B_{11}H_{14}^{-}$.

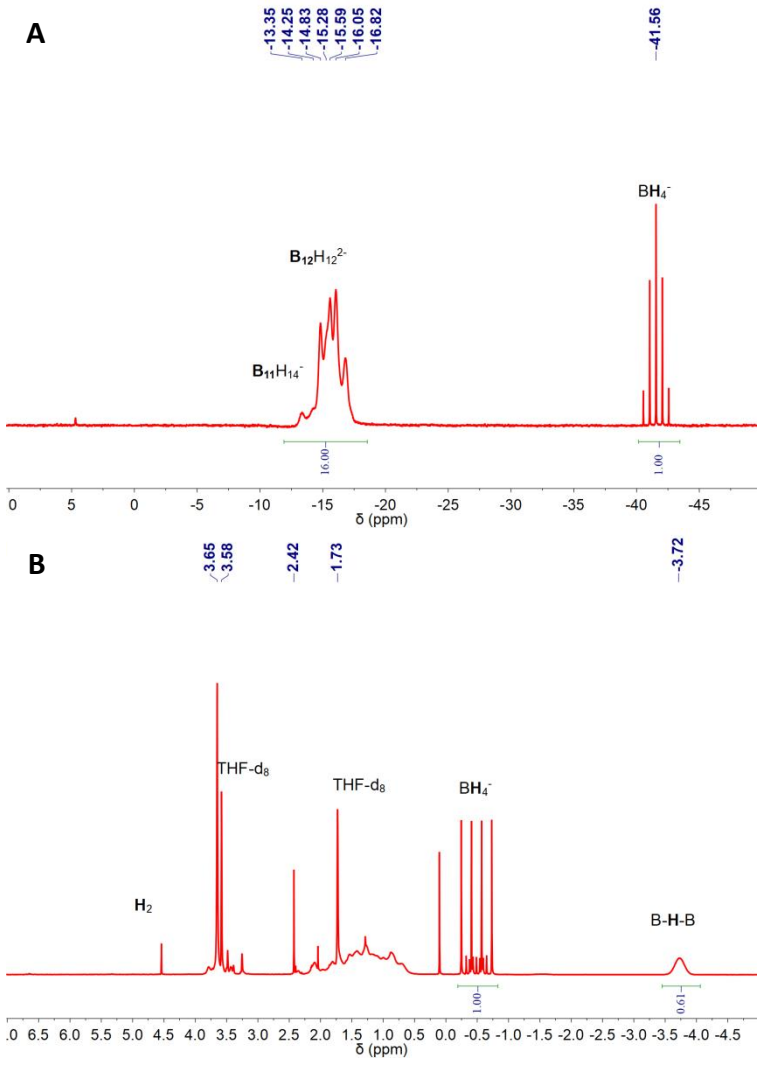

Supplementary Figure 49. (A) Proton-coupled ^{11}B NMR and (B) ^{1}H NMR spectra of solid samples obtained by reaction of 5 mmol ball-milled $LiBH_4$ with 5 equiv (10 % excess) of $DMS{\cdot}BH_3$ for 24 hours at 120°C in toluene in a Schlenk setup. Samples were dissolved in THF-d_8.

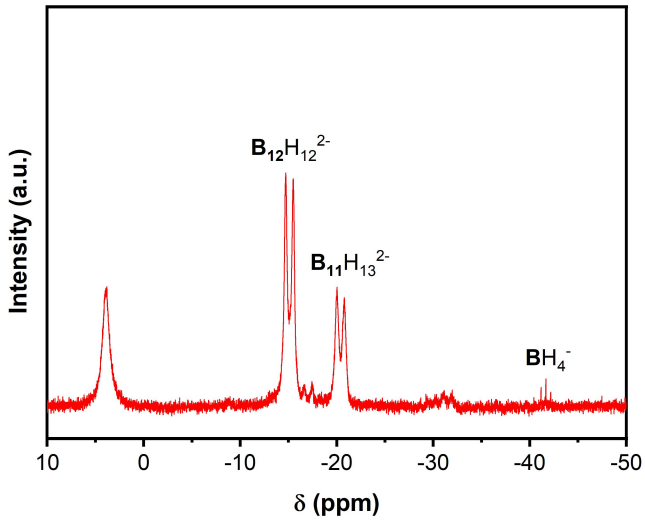

Supplementary Figure 50. Proton-coupled ^{11}B NMR spectra of solid samples obtained by reaction of 5 mmol ball-milled $LiBH_4$ with 5 equiv (10 % excess) of $DMS{\cdot}BH_3$ for 60 hours at 120°C in toluene in a Schlenk setup, upon washing with an excess of THF.

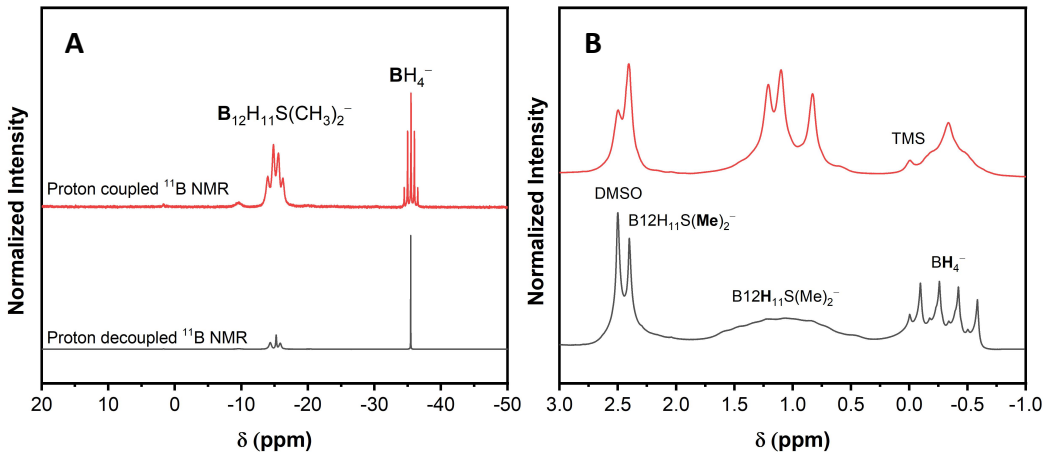

Supplementary Figure 51. (A) Proton-coupled and decoupled ^{11}B NMR and (B) ^{1}H and $^{1}H\{^{11}B\}$ NMR spectra of solid samples obtained by reaction of 5 mmol ball-milled $NaBH_4$ with 27.5 mmol (10% excess) of $DMS{\cdot}BH_3$ in 20 ml toluene for 24 hours at 120°C in a Schlenk flask.

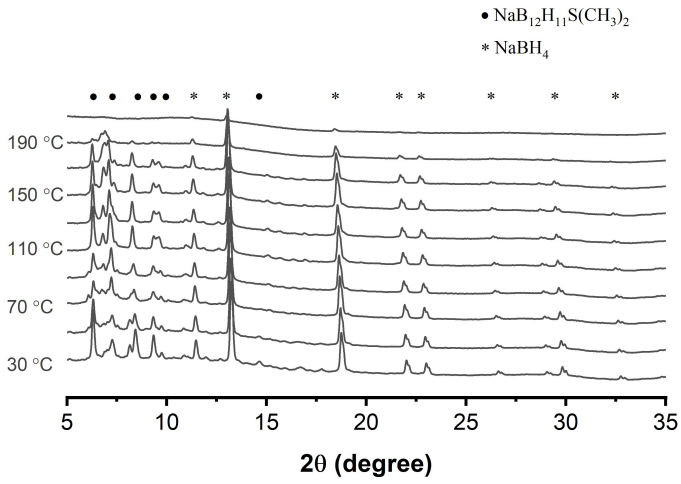

Supplementary Figure 52. In situ variable temperature powder X-ray diffraction data of solid samples obtained by reaction of 5 mmol ball-milled $NaBH_4$ with 27.5 mmol (10% excess) of $DMS{\cdot}BH_3$ in 20 ml toluene for 24 hours at 120°C in a Schlenk flask (λ = 0.71073 Å).

12 Isolation of $B_{11}H_{14}^-$

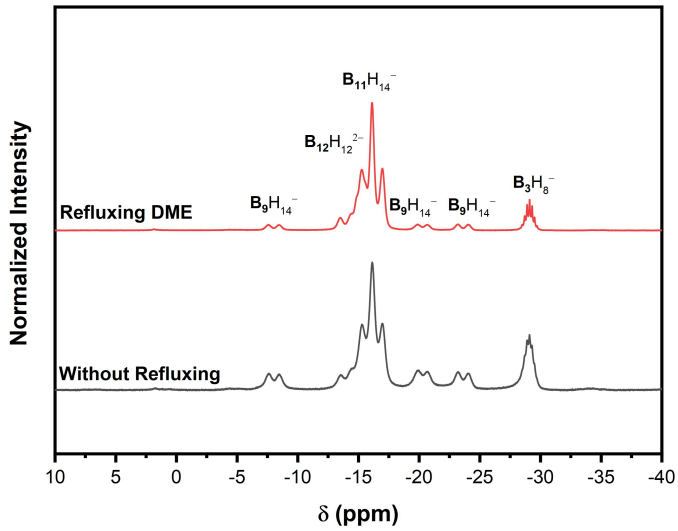

Supplementary Figure 53. Proton-coupled ^{11}B NMR spectra of mixtures obtained by reacting $LiBH_4$ and 10 equiv. $DMS{\cdot}BH_3$ in 20 ml monoglyme in a Schlenk flask without (black curve) or equipped with (red curve) a condenser.

For the isolation of $B_{11}H_{14}^-$, our initial approach involved condensing $LiBH_4$ with $DMS{\cdot}BH_3$ in various ethereal solvents at 85 °C. Our first attempt involved reacting $LiBH_4$ with 10 equivalents of $DMS{\cdot}BH_3$ in monoglyme in a Schlenk setup for 24 hours. Afterward, the free monoglyme was removed *via* a vacuum line at ambient temperature (Supplementary Figure 53). We then added 10 ml of water to the resulting sticky yellow compound, adjusted the pH to below 4 by gradually adding 3 M HCl to convert of $B_3H_8^-$ to boric acid, and extracted the $B_{11}H_{14}^-$ salts by adding 20 ml of diethyl ether to the aqueous solution, as described previously. [20] However, the extracted $B_{11}H_{14}^-$ (Supplementary Figure 54) was in a hydrated form, with a small amount of $B_9H_{14}^-$. The complete removal of $B_9H_{14}^-$ from $B_{11}H_{14}^-$ is challenging due to their similar chemical properties.

In a second attempt, $THF{\cdot}BH_3$ was used instead of $DMS{\cdot}BH_3$, as it is known to have higher activity and selectivity. [21] In this experiment (Supplementary Figure 55), we reacted $LiBH_4$ with 10 equivalents of $THF{\cdot}BH_3$ in an autoclave at 85 °C. This reaction exhibited much higher selectivity for $B_{11}H_{14}^-$ formation. However, the conversion of $THF{\cdot}BH_3$ was incomplete, due to partial transformation into complicated positive oxyborates.[21]

The last methodology involved heat-treatment of the filtrates obtained from our

synthesis of $B_{12}H_{12}^{2-}$. Indeed, we found that the remaining amount of $B_3H_8^-$ in the filtrate was higher than that of $B_9H_{14}^-$ in the solution. Since $B_9H_{14}^-$ not only contributes to $B_{11}H_{14}^-$ formation via hydroboration, but also acts as an intermediate for $B_{12}H_{12}^{2-}$, this approach was used to separate $B_9H_{14}^-$ from $B_{11}H_{14}^-$ by precipitating it out as $Li_2B_{12}H_{12}$ taking advantage of the excess $B_3H_8^-$ in the solution. We thus further heat-treated the filtrate, obtained after reacting $LiBH_4$ with 5 equivalents (10% excess) of DMS·BH_3 at 120 °C for 24 hours, at 160 °C for another 4 hours. This treatment led to the quantitative conversion of $B_3H_8^-$ and $B_9H_{14}^-$ into $B_{12}H_{12}^{2-}$ (Supplementary Figure 56A), which could be separated by a second filtration, leaving $B_{11}H_{14}^-$ (Supplementary Figure 56B) as the main boron species in the solution. Similarly, heat-treating the filtrate obtained from reacting $LiBH_4$ with 10 equivalents of DMS·BH_3 at 85 °C in diglyme for 24 hours at 160 °C for 4 hours resulted in a second conversion of $B_3H_8^-$ and $B_9H_{14}^-$ into $B_{12}H_{12}^{2-}$, leaving $B_{11}H_{14}^-$ as the predominant species in the solution (Supplementary Figure 57).

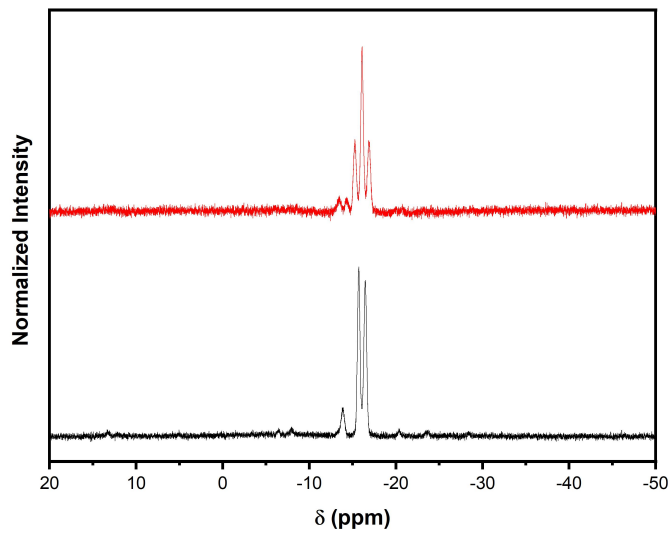

Supplementary Figure 54. Proton-decoupled (black) and coupled (red) ^{11}B NMR spectra of the diethyl ether layer obtained after liquid-liquid extraction of an aqueous solution of diglyme solvated $Li_2B_{12}H_{12}$ at pH = 4.

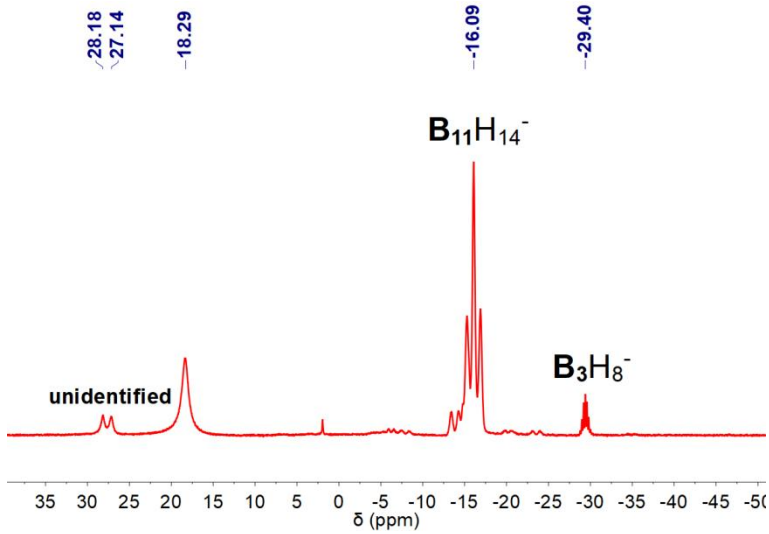

Supplementary Figure 55. Proton-coupled ^{11}B NMR spectrum of the mixture obtained upon reacting $LiBH_4$ with 10 equiv. of $THF{\cdot}BH_3$ in an autoclave at 85 °C for 24 h.

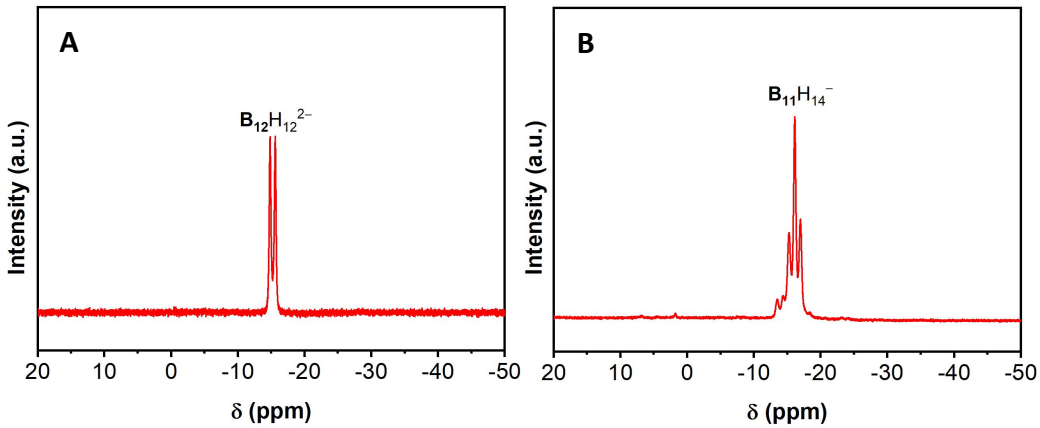

Supplementary Figure 56. Proton-coupled ^{11}B NMR spectra of (A) solid precipitate and (B) reaction solution obtained by heat treatment at 160 °C for 4 h of the filtrate obtained after reaction of $LiBH_4$ with 5 equiv. (10% excess) $DMS{\cdot}BH_3$ in diglyme.

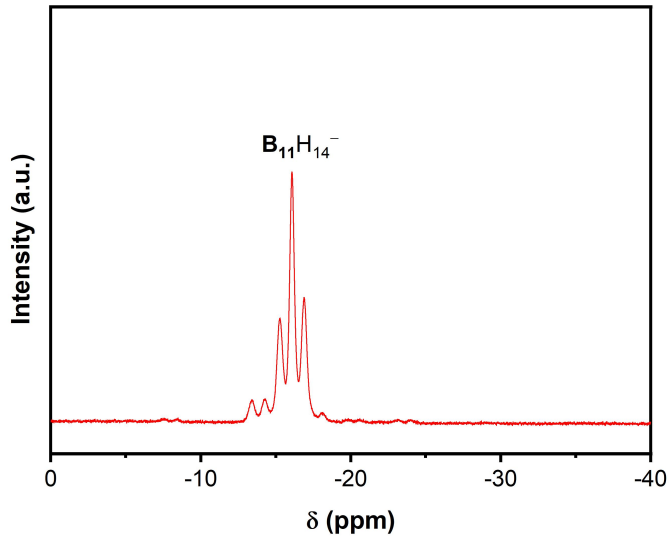

Supplementary Figure 57. Proton-coupled ^{11}B NMR spectrum of solution obtained by heat treatment at 160°C for 4 h of the filtrate obtained after reacting $LiBH_4$ with 10 equiv $DMS{\cdot}BH_3$ in diglyme at 85°C for 24 h.

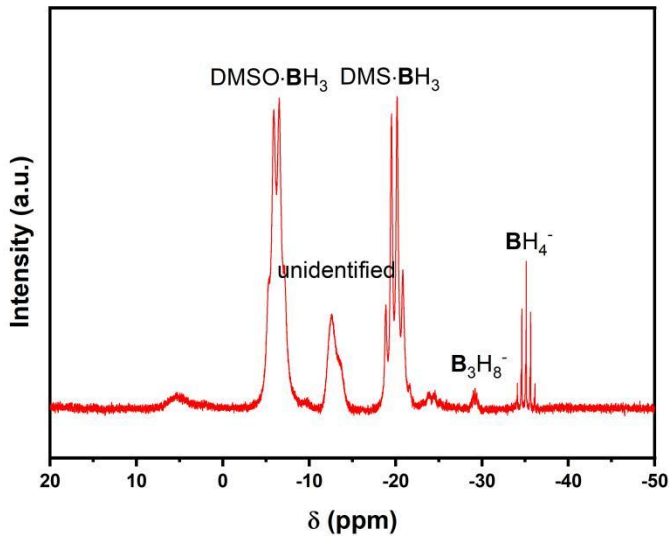

Supplementary Figure 58. Proton-coupled ^{11}B NMR spectrum of solution obtained by heat treatment 27.5mmol $DMS{\cdot}BH_3$ in 20 ml diglyme at 120°C.

13 Crystallographic information

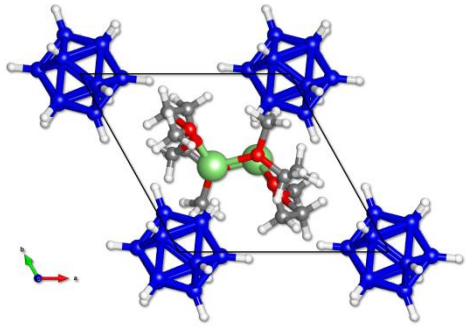

Supplementary Figure 59. Crystal structure fragment of $Li_2B_{12}H_{12}$·2 diglyme

Supplementary Table 9. Crystal data and structure refinement for $Li_2B_{12}H_{12}$·2 diglyme.

Identification code	$Li_2B_{12}H_{12}$·2 diglyme
Empirical formula	$C_6H_{20}B_6LiO_3$
Formula weight	212.02
Temperature (K)	150(2)
Wavelength (Å)	0.71073
Crystal system	Triclinic
Space group	*P*-1
Unit cell dimensions (Å,°)	a = 8.5691(12) b = 9.3870(9) c = 9.7731(10) = 118.061(10) = 90.881(12) = 115.069(14)
Volume ($Å^3$)	605.28(15)
Z	2
Density (calculated) (g/cm^3)	1.163
Absorption coefficient (mm^{-1})	0.073
F(000)	226
Crystal size (mm^3)	0.15x 0.15 x 0.09
Theta range for data collection (°)	3.138 to 26.174
Reflections collected	10377
Independent reflections	2409 [$R_{(int)}$ = 0.0400]
Completeness to q = 25.242° (%)	99.6
Absorption correction	Semi-empirical from equivalents
Max. and min. transmission	1.00000 and 0.89753
Refinement method	Full-matrix least-squares on F^2
Data / restraints / parameters	2409 / 0 / 165
Goodness-of-fit on F^2	1.062
Final R indices [I>2s(I)]	R_1 = 0.0359, wR_2 = 0.0861
R indices (all data)	R_1 = 0.0456, wR_2 = 0.0904
(max,min)($e.Å^{-3}$)	0.220, -0.182

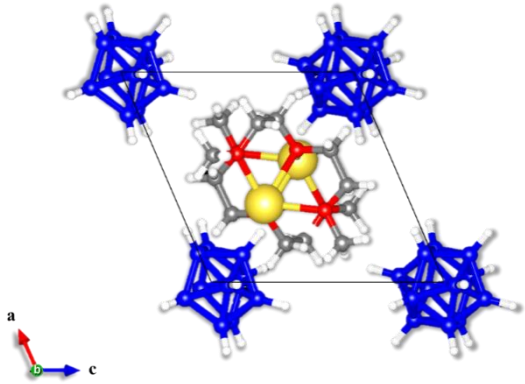

Supplementary Figure 60. Crystal structure fragment of $Li_2B_{12}H_{12}\cdot 1.5$ monoglyme

Supplementary Table 10. Crystal data and structure refinement for $Li_2B_{12}H_{12}\cdot$ 1.5 monoglyme.

Identification code	$Li_2B_{12}H_{12}\cdot 1.5$monoglyme
Empirical formula	$C_6H_{21}B_6LiO_3$
Formula weight	213.03
Temperature (K)	150(2)
Wavelength (Å)	0.71073
Crystal system	Monoclinic
Space group	I2/a
Unit cell dimensions (Å,°)	a = 16.480(5) b = 10.115(2) c = 17.144(5) = 90 = 113.35(3) = 90
Volume ($Å^3$)	2624.0(13)
Z	8
Density (calculated) (g/cm^3)	1.078
Absorption coefficient (mm^{-1})	0.068
F(000)	912
Crystal size (mm^3)	0.18x 0.10 x 0.05
Theta range for data collection (°)	3.131 to 21.257
Reflections collected	5062
Independent reflections	1458 [$R_{(int)}$ = 0.0936]
Completeness to q = 21.257° (%)	99.6
Absorption correction	Semi-empirical from equivalents
Max. and min. transmission	1.00000 and 0.64350
Refinement method	Full-matrix least-squares on F^2
Data / restraints / parameters	1458 / 0 / 148
Goodness-of-fit on F^2	1.088
Final R indices [I>2s(I)]	R1 = 0.0602, wR2 = 0.0908
R indices (all data)	R1 = 0.0994, wR2 = 0.1005
Dr (max,min)($e.Å^{-3}$)	0.164, -0.153

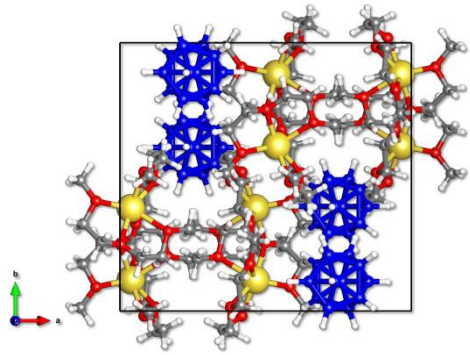

Supplementary Figure 61. Crystal structure fragment of $Na_2B_{12}H_{12}$·4 diglyme

Supplementary Table 11. Crystal data and structure refinement for $Na_2B_{12}H_{12}$·4 diglyme.

Identification code	$Na_2B_{12}H_{12}$·4 diglyme
Empirical formula	$C_{12}H_{34}B_6NaO_6$
Formula weight	362.24
Temperature (K)	150(2)
Wavelength (Å)	0.71073
Crystal system	Monoclinic
Space group	*I*2/*a*
Unit cell dimensions (Å,°)	a = 17.4862(17) b = 14.6333(9) c = 17.7938(19) = 90 = 114.360(12) = 90
Volume ($Å^3$)	4147.7(8)
Z	8
Density (calculated) (g/cm^3)	1.160
Absorption coefficient (mm^{-1})	0.098
F(000)	1560
Crystal size (mm^3)	0.480x 0.350 x 0.300
Theta range for data collection (°)	3.506 to 26.507
Reflections collected	4138
Independent reflections	4138 [$R_{(int)}$ = /]†
Completeness to q = 25.242° (%)	98.8
Absorption correction	Semi-empirical from equivalents
Max. and min. transmission	1.00000 and 0.50355
Refinement method	Full-matrix least-squares on F^2
Data / restraints / parameters	4138 / 0 / 249
Goodness-of-fit on F^2	1.081
Final R indices [I>2s(I)]	R_1 = 0.0676, wR_2 = 0.1691
R indices (all data)	R_1 = 0.0824, wR_2 = 0.1833
(max,min)($e.Å^{-3}$)	0.331, -0.360

† The crystal was twinned and refined against HKLF5 formatted data, imposing MERGE 0

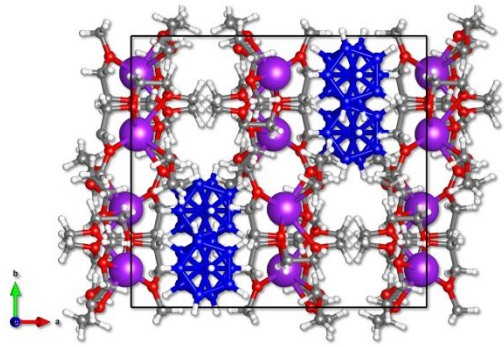

Supplementary Figure 62. Crystal structure fragment of $K_2B_{12}H_{12}$·4 diglyme

Supplementary Table 12. Crystal data and structure refinement for $K_2B_{12}H_{12}$·4 diglyme.

Identification code	$K_2B_{12}H_{12}$·4 diglyme
Empirical formula	$C_{24}H_{68}B_{12}K_2O_{12}$
Formula weight	756.70
Temperature (K)	150(2)
Wavelength (Å)	0.71073
Crystal system	Monoclinic
Space group	*I*2/*a*
Unit cell dimensions (Å,°)	a = 18.627(2) b = 14.8544(10) c = 17.877(2) = 90 = 119.475(17) = 90
Volume ($Å^3$)	4306.2(10)
Z	4
Density (calculated) (g/cm^3)	1.167
Absorption coefficient (mm^{-1})	0.268
F(000)	1624
Crystal size (mm^3)	0.28x 0.11 x 0.02
Theta range for data collection (°)	2.582 to 26.395
Reflections collected	5525
Independent reflections	5525 [$R_{(int)}$ = ?] †
Completeness to q = 25.242° (%)	97.5
Absorption correction	Semi-empirical from equivalents
Max. and min. transmission	1.00000 and 0.69426
Refinement method	Full-matrix least-squares on F^2
Data / restraints / parameters	5525 / 0 / 231
Goodness-of-fit on F^2	0.994
Final R indices [I>2s(I)]	R_1 = 0.0548, wR_2 = 0.1235
R indices (all data)	R_1 = 0.0831, wR_2 = 0.1314
(max,min)($e.Å^{-3}$)	0.429, -0.274

† The crystal was twinned and refined against HKLF5 formatted data, imposing MERGE 0

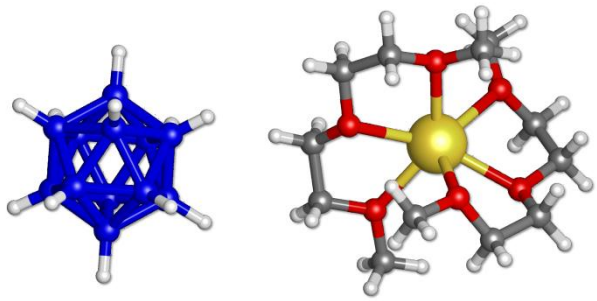

Supplementary Figure 63. Crystal structure fragment of $Li_2B_{12}H_{12}$·2 diglyme

Supplementary Table 13. Crystal data and structure refinement for $Na_2B_{12}H_{12}$·2 diglyme.

Identification code	$Na_2B_{12}H_{12}$·2 diglyme
Empirical formula	$C_{12}H_{40}B_{12}Na_2O_6$
Formula weight	456.14
Temperature (K)	150(2)
Wavelength (Å)	0.71073
Crystal system	Triclinic
Space group	P-1
Unit cell dimensions (Å,°)	a = 9.098(2) b = 9.165(3) c = 9.536(2) = 114.66(3) = 104.47(2) = 105.02(3)
Volume ($Å^3$)	637.3(4)
Z	1
Density (calculated) (g/cm^3)	1.189
Absorption coefficient (mm^{-1})	0.105
F(000)	242
Crystal size (mm^3)	0.30x 0.09 x 0.04
Theta range for data collection (°)	3.669 to 20.837
Reflections collected	1191
Independent reflections	1191 [$R_{(int)}$ = ?]
Completeness to q = 20.837° (%)	88.8
Absorption correction	Semi-empirical from equivalents
Max. and min. transmission	1.00000 and 0.14822
Refinement method	Full-matrix least-squares on F^2
Data / restraints / parameters	1191 / 51 / 148
Goodness-of-fit on F^2	1.081
Final R indices [I>2s(I)]	R1 = 0.1091, wR2 = 0.2672
R indices (all data)	R1 = 0.1347, wR2 = 0.2834
Dr (max,min)($e.Å^{-3}$)	0.692, -0.548

REFERENCES

1. Wang, J.; Steenhaut, T.; Li, H.-W.; Filinchuk, Y. High yield autoclave synthesis of pure $M_2B_{12}H_{12}$ (M = Na, K). *Inorg. Chem.* **2023**, *62* (5), 2153–2160. https://doi.org/10.1021/acs.inorgchem.2c03810
2. Hagemann, H.; Černý, R. Synthetic approaches to inorganic borohydrides. *Dalton Trans.* **2010**, *39*(26), 6006–6012. https://doi.org/10.1039/B927002G
3. Pitochelli, A. R.; Hawthorne, F. M. The isolation of the icosahedral $B_{12}H_{12}^{2-}$ ion. *J. Am. Chem. Soc.* **1960**, *82*, 3228. https://doi.org/10.1021/ja01497a069
4. Miller, H. C.; Miller, N. E.; Muetterties, E. L. Chemistry of boranes. XX. Syntheses of polyhedral boranes. *Inorg. Chem.* **1964**, *3*(10), 1456–1463. https://doi.org/10.1021/ic50020a026
5. Yan, Y.; Remhof, A.; Rentsch, D.; Züttel, A. The role of $MgB_{12}H_{12}$ in the hydrogen desorption process of $Mg(BH_4)_2$. *Chem. Commun.* **2015**, *51*, 700. https://doi.org/10.1039/C4CC05266H
6. Yan, Y.; Rentsch, D.; Battaglia, C.; Remhof, A. Synthesis, stability and Li-ion mobility of nanoconfined $Li_2B_{12}H_{12}$. *Dalton Trans.* **2017**, *46*(37), 12434–12437. https://doi.org/10.1039/C7DT02946B
7. Miller, H. C.; Miller, N. E.; Muetterties, E. L. Synthesis of polyhedral boranes. *J. Am. Chem. Soc.* **1963**, 85 (23), 3885–3886. https://doi.org/10.1021/ja00906a033
8. He, L.; Li, H.-W.; Hwang, S.-J.; Akiba, E. Facile solvent-free synthesis of anhydrous alkali metal dodecaborate $M_2B_{12}H_{12}$ (M = Li, Na, K). *J. Phys. Chem. C* **2014**, *118*, 6084. https://doi.org/10.1021/jp500253k
9. He, L.; Li, H.-W.; Tumanov, N.; Filinchuk, Y.; Akiba, E. Facile synthesis of anhydrous alkaline earth metal dodecaborates $MB_{12}H_{12}$ (M = Mg, Ca) from $M(BH_4)_2$. *Dalton Trans.* **2015**, *44*, 15882. https://doi.org/10.1039/C5DT02343B
10. He, L.; Shao, H.; Felderhoff, M. et al. Facile synthesis of anhydrous $Li_2B_{12}H_{12}$ with high purity by solvent-free method. *Inorg. Chim. Acta* **2017**, *464*, 147–151. https://doi.org/10.1016/j.ica.2017.05.025
11. Han, H.; Liu, X.-R.; Gao, Y.-M. et al. An Improved Method for the Synthesis of $M_2[B_{12}H_{12}]$ (M = Na, K) and Their Formation Mechanism. *Inorg. Chem.* **2024**, *63* (30), 13886–13892. https://doi.org/10.1021/acs.inorgchem.4c00945
12. Bykov, A. Yu.; Mal'tseva, N. N.; Generalova, N. B.; et al. Reactions of sodium tetrahydroborate with alkyl and aryl halides: A new approach to the synthesis of

$B_3H_8^-$ and $B_{12}H_{12}^{2-}$ anions. *Russ. J. Inorg. Chem.* **2013**, *58*(11), 1321–1323. https://doi.org/10.1134/S003602361311003X

13. Geis, V.; Guttsche, K.; Knapp, C.; Scherer, H.; Uzun, R. Synthesis and characterization of synthetically useful salts of the weakly-coordinating dianion $[B_{12}Cl_{12}]^{2-}$. *Dalton Trans.* **2009**, *15*, 2687. https://doi.org/10.1039/B821030F
14. Chen, W.; Wu, G.; He, T.; Li, Z.; Guo, Z.; Liu, H.; Huang, Z.; Chen, P. An improved synthesis of unsolvated NaB_3H_8 and its application in preparing $Na_2B_{12}H_{12}$. *Int. J. Hydrogen Energy* **2016**, *41*(34), 15471–15476. https://doi.org/10.1016/j.ijhydene.2016.02.143
15. Pylypko, S.; Ould-Amara, S.; Zadick, A. et al. The highly stable aqueous solution of sodium dodecahydro-closo-dodecaborate $Na_2B_{12}H_{12}$ as a potential liquid anodic fuel. *Appl. Catal. B* **2018**, *222*, 1. https://doi.org/10.1016/j.apcatb.2017.09.068
16. Jing, Y.; Wang, X.; Han, H. et al. Selective synthesis of the $B_{11}H_{14}^-$ and $B_{12}H_{12}^{2-}$ borane derivatives and the general mechanisms of the B–H bond condensation. *Sci. China Chem.* **2023**, *66*(7), 876–881. https://doi.org/10.1007/s11426-023-1852-9
17. He, L.; Li, H.-W.; Akiba, E. Thermal decomposition of anhydrous alkali metal dodecaborates $M_2B_{12}H_{12}$ (M = Li, Na, K). *Energies* **2015**, *8*(11), 12429–12438. https://doi.org/10.3390/en81112326
18. Remhof, A.; Yan, Y.; Rentsch, D.et al. Solvent-free synthesis and stability of $MgB_{12}H_{12}$. *J. Mater. Chem. A* **2014**, *2*(20), 7244–7249. https://doi.org/10.1039/C4TA00644E
19. Hamilton, E. J. M.; Jordan, R.; Meyers, E. A.; Shore, S. G. One-step preparation of dimethyl sulfide substituted icosahedral boranes: The crystal and molecular structures of 1,7-$(SMe_2)_2B_{12}H_{10}$, 1,12-$(SMe_2)_2B_{12}H_{10}$, and $[SMe_3][B_{12}H_{11}(SMe_2)]$·MeCN. *Inorg. Chem.* **1996**, *35*(18), 5335–5341. https://doi.org/10.1021/ic960433w
20. Souza, D. H. P.; Møller, K. T.; Moggach, S. A.et al. Hydrated alkali-$B_{11}H_{14}$ salts as potential solid-state electrolytes. *J. Mater. Chem. A* **2021**, *9*, 15027–15034. https://doi.org/10.1039/D1TA01551F
21. Lane, C. F. Reduction of organic compounds with diborane. *Chem. Rev.* **1976**, *76*(6), 773–799. https://doi.org/10.1021/cr60304a005